A Heuristic Optimization Approach to Hydrodynamic Wave Energy Converter Geometry

Kaylie McTiernan

A thesis

submitted in partial fulfillment of the

requirements for the degree of

Master of Science in Mechanical Engineering

University of Washington

2018

Reading Committee:

Benjamin Maurer, Chair

Tim Mundon

Bryony DuPont

Alberto Aliseda

Brian Fabien

Program Authorized to Offer Degree:

Mechanical Engineering Department

University of Washington

Abstract

A Heuristic Optimization Approach to Hydrodynamic Wave Energy Converter Geometry

Kaylie McTiernan

Chair of the Supervisory Committee:
Benjamin Maurer, Senior Mechanical Engineer and Affiliate Assistant Professor
Applied Physics Lab and Mechanical Engineering

Ocean waves are an abundant global resource that can be converted to mechanical and electrical power. Modern research on wave energy conversion began in the 1970s, with many types of wave energy converter designs under active development. Optimizing the design of wave energy converters to enhance power production is crucial for lowering their cost of energy. In this study we present a heuristic optimization method to optimize wave energy hull shapes for power output. We use a computationally efficient genetic algorithm leveraging frequency domain analysis and model simplifications. Central to this research is the development of a simplified proxy to estimate system power based on the frequency domain hydrodynamic coefficients.
As a case study, this method is applied to the miniWEC two-body point absorber to optimize its axisymmetric hull shape for a Lake Washington wave climate. A genetic algorithm is run for 100

generations and identifies a hull shape that has three times the average power as compared to the existing miniWEC system. The results are promising and indicate that this method may be useful for other research studies, and especially for commercial wave energy applications where power production and cost of energy are crucial to development.

TABLE OF CONTENTS

LIST OF FIGURES

LIST OF TABLES

ACKNOWLEDGEMENTS

I would like to thank my committee members for their guidance and expertise, without which this research would not be possible. Thanks to the Applied Physics Lab miniWEC developers including Professor Jim Thompson for supporting this work and for providing Lake Washington wave data. Also, for the opportunity to participate in miniWEC testing in January 2018. Thanks to Curty Rusch for sharing his miniWEC ProteusDS model for use in this research, and for providing guidance in this area. Thanks to Brian Rosenberg for NEMOH guidance and frequency-domain power equations. Rob Cavagnaro and James Joslin also provided insight into ProteusDS and the reference hull shape analysis. Thanks to the developers of NEMOH, as the code has been crucial in this research. Thank you to the Clean Energy Institute for providing a travel grant to present this research at the 2018 Marine Energy Technology Symposium in Washington DC. Thank you to Alec Finlay for use of his poem in the introduction.

Chapter 1. INTRODUCTION

be sure that your gear
will get fankled
by mollusks and weed

it's not the median tide
but the storm –
that will finally decide

as the sea is various
no one device
will ever suffice

there are too many
possible settings
for a fitting form
to be settled yet

-Alec Finlay, "after gareth and laura we sometimes used to say…" (lines 46-58) [1]

Renewable energy is needed to mitigate the effects of climate change. Wave energy is a form of renewable energy that harnesses the power of ocean waves, a globally abundant resource collocated with many coastal cities. As renewable energy resources continue to replace traditional electricity sources, there is room for diverse forms of renewable energy to create resilient grid systems. However, further research and development is still needed to make wave energy cost-competitive with other forms of energy. There are many types of wave energy converter concepts under development which harness the kinetic energy in waves to produce mechanical and/or electrical power. Wave energy converter designs are being developed at many locations globally, including a wave energy research platform at the University of Washington.

Wave energy can have a positive impact on society by contributing to a globally abundant, renewable source of energy with a high energy density. There is an estimated 2 Terawatts of wave

energy globally and some of that energy could be harnessed by wave energy converters [2]. Waves build up over time and large distances as a result of wind blowing over the surface of the water, making them a more steady, concentrated energy resource than wind. The highest wave density occurs between the 40th to 60th latitude lines in both the northern and southern hemispheres (Figure 1), which can be a plentiful renewable resource for populations living along ocean coastlines in these regions. Energy from ocean waves can contribute to climate change mitigation and can also have positive local benefits.

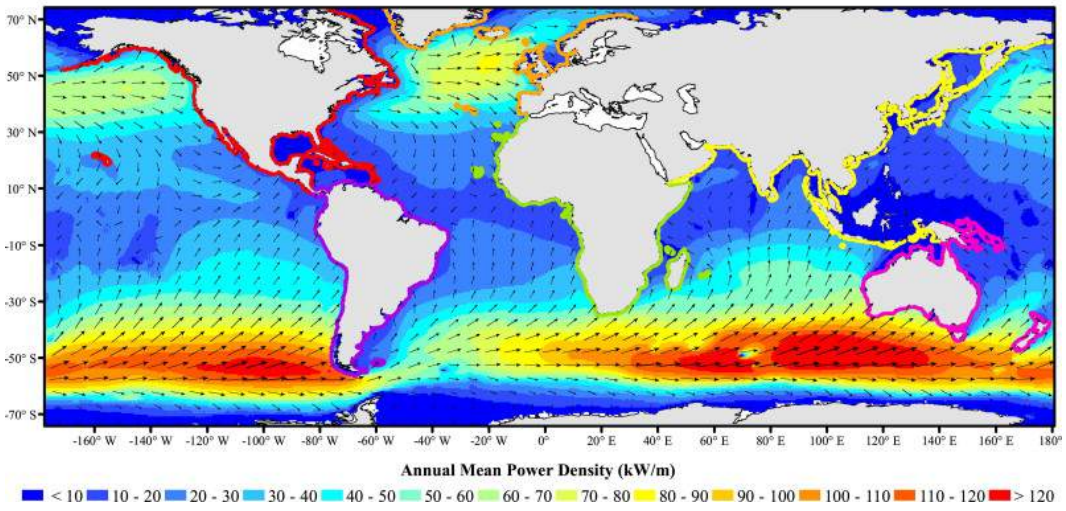

Figure 1 - Global Wave Energy Resource [2]

Wave energy can provide sustainable power and socio-economic benefits to coastal communities. One third of the global population lives within 100 km of the coast [3] and many coastal cities are collocated with a wave resource. Wave energy can provide local jobs and reinvigorate maritime markets. Projects can be designed for small communities, larger population centers, or other markets including water desalination, autonomous underwater vehicles, ports, and

aquaculture. Wave energy projects can be designed with local communities in mind, as there are still many types of wave energy converters.

Wave energy converters harness the kinetic energy of waves, and typically convert this to electrical power. Many types of wave energy converters have been proposed including devices located offshore, nearshore, and onshore [5]. Energy can be harnessed from the vertical motion of deep water waves, the horizontal motion of intermediate depth and shallow water waves, variations in pressure, and variations in wave height, among others. Diversity of wave energy converter design reflects the variation of wave resource at different sites globally.

Research and development can reduce the cost of wave energy to make it cost competitive with conventional energy sources. There are many engineering challenges, especially generating cost effective power in typical wave conditions, while also being able to survive in harsh storm conditions [6]. Wave energy technical and economic advancements are ongoing globally, and research on power optimization are key to this aim.

1.1 BACKGROUND

Wave energy converters can be better understood through the physics of oscillating systems in ocean waves, the variation in wave energy designs, analysis methods, and the means through which these devices have been optimized. Linear wave equations provide the foundation of wave energy converters models. There are many types of wave energy converters which can be analyzed in both the frequency domain and the time domain. Optimizing the performance of wave energy converters is currently an active area of research.

1.1.1 *Linear Wave Theory*

Linear wave theory is a simplified physical description of ocean waves that can be used for ocean engineering. Real sea states have complex dynamics, but linear wave theory describes the basic physical processes well, especially for waves of small amplitude relative to the water depth [7].

Wave energy converters interact with the waves as oscillating systems [8-9]. Equation 1.1 is the equation of motion for a heaving point absorber of mass, m, and displacement, $X_{(t)}$ [9-10]. The total force, $F_{T(t)}$, has components of fluid induced forces, $F_{F(t)}$, and external forces, $F_{EXT(X,\dot{X},t)}$.

$$m\ddot{X} = F_{T(t)} + F_{EXT(X,\dot{X},t)} \tag{1.1}$$

The fluid-induced forces, $F_{F(t)}$, can be approximated using linear wave theory by the sum of the exciting, radiating, and hydrostatic forces: $F_{Ex(t)}$, $F_{R(t)}$, and $F_{H(t)}$, respectively (Equation 1.2).

$$F_{F(t)} = F_{Ex(t)} + F_{R(t)} + F_{H(t)} \tag{1.2}$$

Each of the terms have components in six degrees of freedom (Heave [z], Surge [x], Sway [y], Roll [rx], Pitch [ry], and yaw [rz]). The exciting force is proportional to the incident wave amplitude [11]. The radiating force component includes the added mass and damping coefficients. Finally, the hydrostatic forces are exerted on the submerged body. All these terms form the foundation of hydrodynamic wave energy analysis, which can be used in either the time domain or the frequency domain.

The wave elevation $\eta_{(x,t)}$ is given by equation 1.3 [8]. The signal is evaluated in the frequency domain, where ω is the angular frequency in radians per seconds and β is the angle between the incoming wave and the x axis.

$$\eta_{(x,t)} = Acos\big(k\big(xcos(\beta) + ysin(\beta)\big) - \omega t\big) = Re\big[Ae^{i\left(k(xcos(\beta)+ysin(\beta)-\omega t)\right)}\big] \quad (1.3)$$

Hydrodynamic coefficients can be evaluated in the frequency domain by considering a single frequency at an arbitrary wave angle and assuming linear wave theory [8]. The series of individual sinusoidal waves is valid when the wave amplitude is small. *A* is the wave amplitude, *k* is the wave number which can be determined using the dispersion equation [11], and there are space components *x* and *y* and time *t*. The wave elevation relates to the excitation force by equation 1.4 [12].

$$F_{Ex(t)} = Re\big[A\tilde{F}_{Ex(\omega)}e^{-i\omega t}\big] \quad (1.4)$$

The excitation force includes the complex amplitude of the excitation force $\tilde{F}_{Ex(\omega)}$ in the frequency domain for an incident wave of a given amplitude [11], relating excitation force to the incident wave elevation. Falnes [10] states that in order to efficiently absorb waves, a wave energy converter (WEC) must be a good at generating waves. A WEC can effectively absorb waves by moving with large amplitude and velocity while remaining predominantly in phase with the incoming waves. The ideal phase angle between the incoming waves and a WEC is 90°.

1.1.2 *Wave Energy Converter Types*

There are many types of WEC concepts at various stages of research and development. Modern wave energy research began in the 1970s, and the first known wave energy device dates back to 1799 [13]. Wave energy can be harnessed offshore in deep ocean, nearshore in intermediate and shallow water depths, as well as onshore along the coast. Figure 2 shows many of the WECs currently under research and development, including the attenuator, point absorber, oscillating wave surge converter, oscillating water column, overtopping, and pressure differential WEC types [14]. Each of these devices harnesses wave energy in a different way using the vertical heave, horizontal surge, or lateral sway motions of waves individually or in combination.

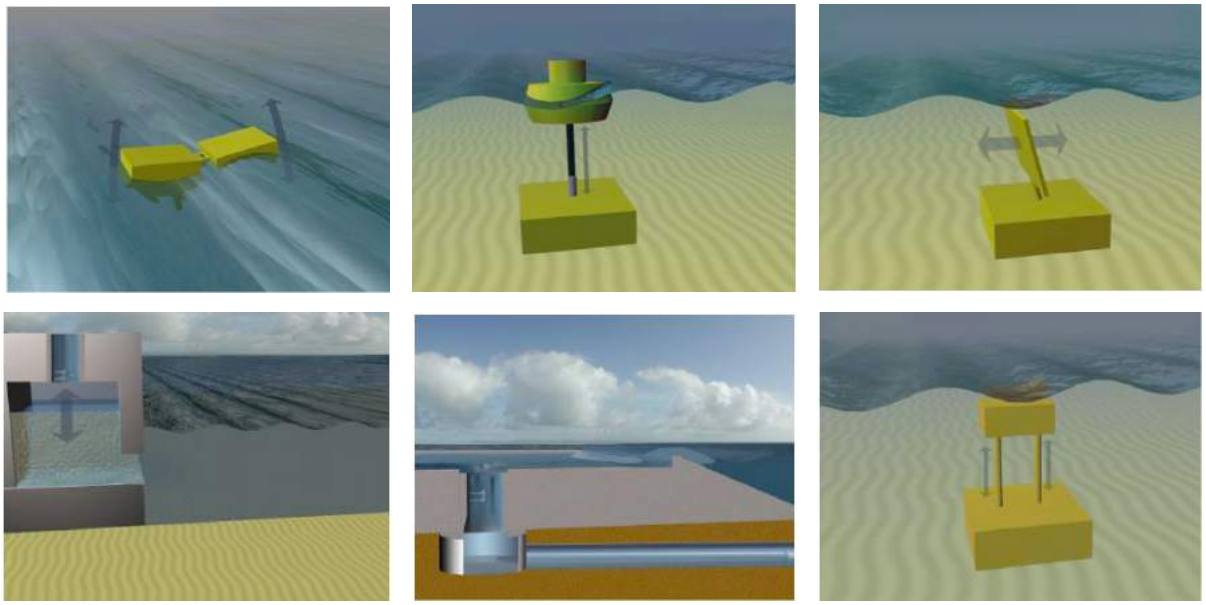

Figure 2 - WEC Types: Attenuator, Point Absorber, Oscillating Wave Surge Converter, Oscillating Water Column, Overtopping, Pressure Differential (top left to bottom right) [14]

Attenuators move on the surface of the water and harness the motion between multiple structural components. Point absorbers are very small relative to the wavelength of incoming

waves, and move on the surface of the water relative to a stationary reference point. The various types of point absorbers will be covered below in further detail. Oscillating wave surge converters operate in intermediate or shallow water depths to oscillate with the horizontal motion of waves near the sea floor [6]. The oscillating water column makes use of the variation in water elevation within a chamber to drive an air turbine. An overtopping device uses the potential energy of waves to generate energy. Finally, the pressure differential device is partially submerged to harness the pressure of waves passing above the device [6].

Over 50% of global wave energy research and development has focused on point absorbers [15], and this research study focuses on a point absorber application. A point absorber is a type of WEC that has a buoyant hull on the surface of the water that moves relative to a stationary reference body. These devices are much smaller than the wavelength of incoming waves, and typically harness heave motion vertically, but can also harness power in up to six degrees of freedom in some variations. The point absorber's stationary body may be the seafloor or alternatively, a submerged structure hanging beneath the hull, with corresponding variations in mooring design.

Point absorbers have been developed and tested at scale in real ocean environments including the CorPower WEC [16], the Oscilla Power Triton [17], the Fred Olson Lifesaver [18], and the Ocean Power Technologies PowerBuoy [19]. The CorPower wave energy converter (Figure 3) is a single body point absorber rigidly connected to the seafloor with one tether. The Oscilla Power Triton (Figure 4) is a two-body point absorber with a submerged reaction structure and multiple (3) tendon connections between the bodies. The hull shape is directional, with shape variation related to the incoming wave direction. The Fred Olson Lifesaver (Figure 5) has an axisymmetric ring shape that has multiple tendons (3) that are connected to the seafloor. The Ocean Power

Technologies PowerBuoy (Figure 6) is an axisymmetric device with a hull design that is similar to a navigation buoy and has a rigid connection between the two bodies. There are a variety of point absorber designs, and the hull geometry of the four shows variation of a round hull, an oblong hull with a narrow bow, a large ring, and an axisymmetric buoy. There is great variation in WEC design, even limiting the focus to point absorbers.

Figure 3 - CorPower Wave Energy Converter [16]

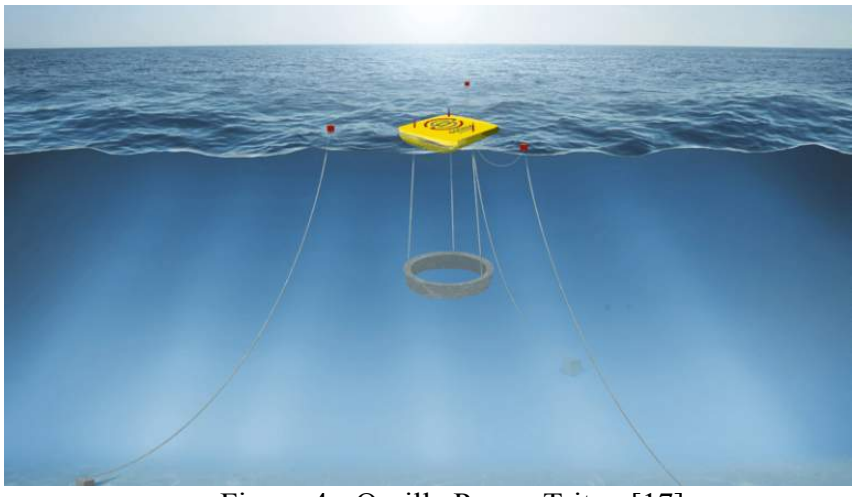

Figure 4 - Oscilla Power Triton [17]

Figure 5 - Fred Olsen Lifesaver [18]

Figure 6 - Ocean Power Technology PowerBuoy [19]

Modern wave energy research and development began in the 1970s, including one of the most notable WEC designs: Salter's Duck [8, 20]. Salter's Duck is a terminator device with an almond shape. Figure 7 shows the Duck being tested in a narrow wave tank. The device can be scaled up by lining up many Duck's side by side perpendicular to the incoming wave direction. Salter's Duck performs with high efficiency in a wave tank with regular waves, but there are greater efficiency losses in real, irregular waves.

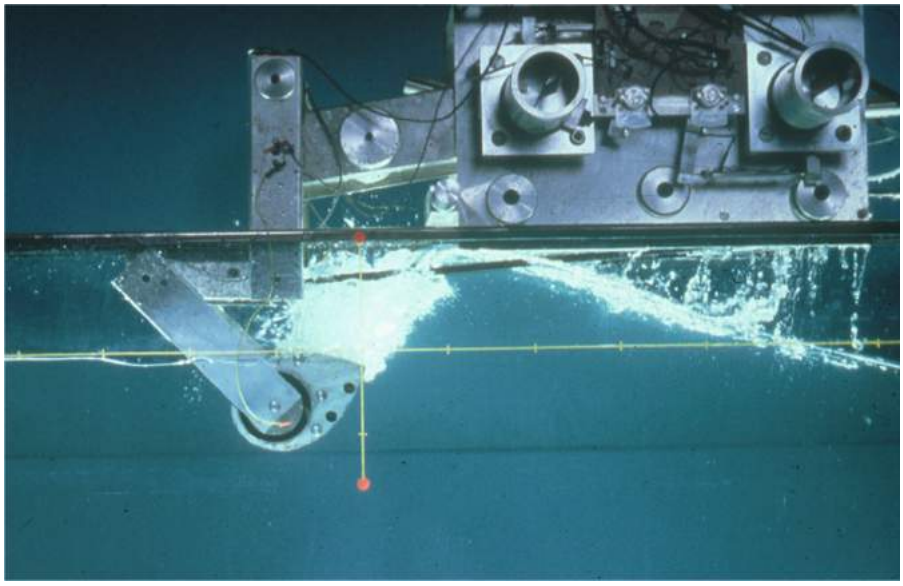

Figure 7 - Salter's Duck Tank Testing [8, 20]

Salter's Duck was developed through a traditional design method of design, test, and iterate, resulting in a wide variety of geometries tested in a wave tank. There are endless design options, as evidenced by that fact that modern wave energy research and development still includes a large variation in design. With such an expansive design space, the traditional design-build-test approach is very expensive and time consuming.

1.1.3 *Frequency Domain Analysis*

Frequency domain analysis of ocean waves and WEC oscillating systems tends to employ boundary element methods (BEM) to solve first-order wave loading on structures. These BEM codes calculate the coefficients of the radiation and excitation forces on hydrodynamic structures, which are used to provide an approximation of the device performance. However, BEM solvers are limited in that they are unable to calculate drag forces which must be determined empirically, experimentally, or through an alternative numerical approach. A number of BEM codes are

available as commercial off-the-shelf software. WAMIT [22-23], and ANSYS AQWA [24] are commercial software packages. NEMOH is an open-source BEM solver developed in Nantes, France [25].

Frequency domain analysis is more computationally efficient than time domain analysis because frequency domain analysis is the Fourier transform of the time domain signal [21]. Convolution in the time domain is equivalent to multiplication in the frequency domain, and thus frequency domain analysis is often used because the Fourier transform and multiplication are much faster than convolution. The time domain and frequency domain analysis for linear, time-invariant behavior are equivalent for finding the post-transient system response. Frequency domain analysis is often used when linear modeling is sufficient, as it is more computationally efficient than time domain analysis.

1.1.4 *Time Domain Analysis*

Time domain analysis evaluates loads on structures during a time interval to model system behavior. There are several dynamic analysis software packages that evaluate engineered ocean structures in the time-domain. These include mid-fidelity simulation packages and high-fidelity computational fluid dynamic codes. The mid-fidelity codes include ProteusDS [26], OrcaFlex [27], and WEC-Sim [28]. The hydrostatic coefficients from the BEM codes are inputted into the time-domain codes. OrcaFlex was developed by a group in the U.K. in the 1980s primarily for the oil and gas sector, and there has been significant development of this commercial code [27]. ProteusDS was developed by a group in Victoria, Canada [26]. This analysis software includes the capability to accurately model the power take-off system of WECs. WEC-Sim is another mid-fidelity time-domain code, which was developed by the National Renewable Energy Laboratory and Sandia National Laboratories [28]. This code runs through MATLAB and is otherwise open-

source to the public. These are only some of the many mid-fidelity time domain codes available, many of which are being validated as part of WEC development standards [29-30].

High fidelity computational fluid dynamics (CFD) codes can be used to get a solution with a higher order of accuracy, with the tradeoff of a much longer run time. There are many high-fidelity CFD codes including ANSYS Fluent and STAR-CCM+ [31-32]. Additionally, OpenFOAM is an open-source CFD code that is often used in ocean engineering research [33]. The time-domain codes can simulate WECs in ocean environments, and analyze the dynamic response of the structures over time. The time-domain codes can be used to determine an annual energy production for WECs in real ocean environments prior to tank testing or field deployments.

1.1.5 *Optimization Approaches*

Geometry optimization approaches may contribute to a significant increase in the annual energy production of WECs. The hull shape of a point absorber can be geometrically optimized to move with greater velocity in ocean waves. Types of geometry optimization methods include direct optimization methods, heuristic optimization methods, and exhaustive search methods. Direct methods use objective functions and solve through a finite sequence of operations. Heuristic optimization methods solve a problem iteratively and strategically in a design space. Heuristic optimization methods may be preferable to direct methods for hydrodynamic WEC geometry optimization because the calculations required for direct methods may not be feasible. Additionally, exhaustive search methods are not practical because the search space is too large, and design and test methods would likely not find an optimized solution.

A genetic algorithm is a type of heuristic optimization method which borrows from the biological process of natural selection [34]. There are ‘populations’ of candidate solutions which are evaluated using an objective function. The candidate solutions are ranked based on their

evaluation, and this determines the GA's search direction over many 'generations'. A genetic algorithm is used in this research because it has been effectively applied to other WEC research studies [38-40].

1.2 Wave Energy Heuristic Optimization Literature

There has been research on the application of genetic algorithms to wave energy optimization, frequency-domain analysis within heuristic methods, and reductions model geometric complexity for design applications. Genetic algorithms (GAs) have been explored in many areas of research, including wave energy. The WEC's geometry, control parameters, mooring layout, or site selection can each be optimized using a GA or another method. Several studies have used frequency domain analysis exclusively within genetic algorithm WEC geometry optimizations.

1.2.1 *Genetic Algorithms Applied to Wave Energy*

Genetic algorithms have been used in wave energy optimization research [35-44]. In particular, genetic algorithms can be used to optimize the control parameters of WECs. Control methods can be used to increase the power extraction in waves by making a device behave in resonance across a range of operational cases. Babarit et al. [35] optimized the control parameters and hull geometry of a floating WEC that behaves like a pendulum. Time-domain and frequency-domain analysis are used within the genetic algorithm to optimize the WEC with active control. Mundon [36] developed a control strategy for the Pelamis WEC by artificially evolving the neurobiological structure of the Lamprey as it has a similar motion to the Pelamis WEC. Gunn et al. [37] optimized a WEC control strategy without prior knowledge of the wave field. Each of these papers implemented a genetic algorithm to incorporate a control strategy for WEC power optimization.

1.2.2 *Frequency Domain Analysis within Genetic Algorithms*

Genetic algorithms have been used to optimize WEC geometry using frequency domain analysis to identify optimized post-transient WEC behavior. Many WEC shape optimization research studies have used frequency domain analysis within heuristic optimization methods. McCabe [38] optimized the hull shape of a submerged WEC that moves in surge horizontally using a bi-cubic B-spline surface between a relatively small number of control points to smooth the shape in 3D space. In McCabe's analysis, the hull shapes were optimized using the frequency-domain code WAMIT [21], as this was the most practical way to obtain the hydrodynamic coefficients. The objective function evaluation included optimal power in addition to shape complexity and size constraints. Garcia-Teruel et al. [39] continued this research with a geometry optimization approach which maximized WEC power and minimized cost of energy; using WAMIT for frequency-domain analysis. Adding time-domain analysis is an area of future work. Gomez et al. [40] optimized the geometry of an oscillating water column using WAMIT for analysis. Sharp et al. [41] used a genetic algorithm with WAMIT frequency-domain analysis to optimize the layout of an array of five WECs. Frequency domain analysis has been effectively used in these studies; further computational efficiency can be increased through model simplifications.

1.2.3 *Reducing Model Complexity within Heuristic Optimization Methods*

Researchers have sought to reduce model complexity within heuristic optimization methods. Ortiz et al. [42] optimized a WEC mooring system using a metamodel based on the pre-processing stage of high fidelity time-domain analysis in order to strategically search the design space of WEC mooring layouts. Bailey et al. [43] optimized a simple pontoon WEC at different sites globally using ProteusDS in the time domain. The simplifications were made to the geometry so that the single dimension of pontoon length was being optimized. This previous research demonstrates the

variation in scale required to optimize a WEC in a specific wave climate. Sale et al. [44] developed a computationally efficient numerical model to optimize the blade shape of a tidal turbine. Reducing model complexity has significant benefits for time-intensive research problems, and similar model simplifications could be used within a GA using frequency domain analysis to enhance computational efficiency.

1.3 THESIS OVERVIEW

This thesis is structured as follows. Chapter 2 presents the methodology and specific WEC case study. A point absorber research platform is evaluated in a specific wave climate. The methodology discussion includes the research scope, development of a proxy for average WEC power, the genetic algorithm method, and the verification steps. Chapter 3 presents the results of this work, including the verification results, the equation developed as a proxy for average power, and the hull shapes identified by the genetic algorithm along with their time domain analysis. Chapter 4 is a discussion of the findings. The significance of the power proxy, effectiveness of the genetic algorithm, strengths and limitations of the methods, computational time, and hull shapes identified are discussed. Chapter 5 discusses the conclusion of the work. The GA code is available on GitHub and presented in the appendix.

Chapter 2. METHODOLOGY

The aim of this work is to investigate the potential for WEC geometry optimization using a genetic algorithm with evaluation in the frequency domain and geometric simplifications. The methodology is a computationally efficient way to identify an optimized WEC hull geometry as compared with the traditional design-build-test method. The optimization approach is applied to a WEC's hull geometry to enhance the average power output in a specific wave climate.

WEC hull geometry is optimized for power production in a specific wave climate by applying a GA with verification steps. Verification steps are included prior to running the GA to understand geometric feature sensitivity within the analysis and to evaluate reference shapes to form the basis of the power proxy. The development of an accurate proxy for power is a central piece of this work. This empirical 'power proxy' is determined based on reference shape analysis. The reference shapes are evaluated in the frequency domain and the time domain to obtain an equation that relates power to the frequency domain hydrodynamic coefficients. The coefficients are weighted and summed to obtain the proxy for power, and this work will be discussed in the optimization approach in Section 2.2. The GA is run over 100 generations, and the final shape in addition to an intermediate shape are evaluated in the time domain. Time domain analysis is not required within the GA but is useful during these verification steps to ensure that the GA is identifying a hull shape with enhanced power performance.

A computationally efficient method is important for practical design applications and reducing model complexity can further this aim. The hull model is simplified by considering axisymmetric geometry, considering vertical heave motion exclusively, and by evaluating in the frequency domain rather than the time domain. The hull shape is axisymmetric, and the submerged volume of each candidate shape is equivalent to maintain constant mass. The geometric search space is defined as a 2D profile slice of the 3D axisymmetric shape. The shape can vary between a minimum and maximum radius over a defined height. The search space increments are able to be relatively fine over the 2D hull profile between these bounds. The two-body point absorber used in the case study primarily produces power in heave motion vertically, and thus only the heave component optimization is included as a simplification. As discussed previously, frequency domain analysis is more computationally efficient than time domain analysis and obtains an

equivalent result for a linear, time-invariant system. Various tools make reducing model complexity possible including a frequency domain code, a genetic algorithm code, and a time domain solver which are all compatible with MATLAB. These tools that enable a computationally efficient method are elaborated upon in the WEC case evaluation section which presents the specific WEC used to test the methodology.

2.1 MiniWEC Case Evaluation: Axisymmetric Hull in Lake Washington

As a way of validating the results of this work and as a way of keeping the research in the realm of the practical, the method is applied to a specific WEC and wave climate. We plan to use the real WEC as a demonstration platform for the methodology to showcase the WEC hull geometric optimization for power performance. Specifically, the axisymmetric hull shape of the miniWEC two-body point absorber is optimized for average power in Lake Washington, shown in Figure 8.

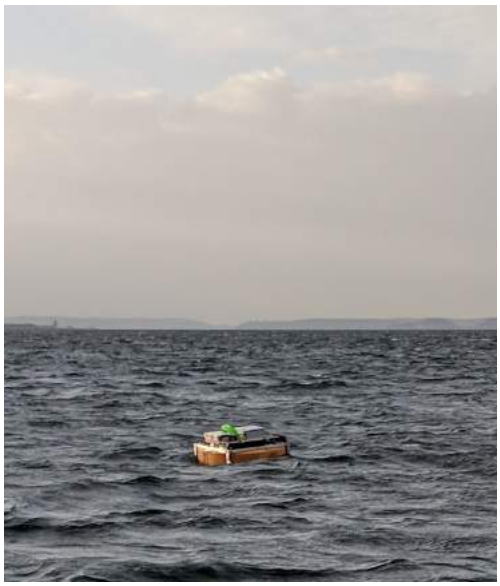

Figure 8 - miniWEC During Testing in Jan 2018

The miniWEC in Lake Washington serves as a 1:7 scale testbed for a full-scale WEC in an open ocean environment. The case evaluation includes presentation of the tools used and the specific Lake Washington wave resource and miniWEC point absorber.

2.1.1 *Lake Washington Wave Resource*

Lake Washington is a freshwater lake near Seattle, WA. The large lake was previously connected to the ocean through the Duwamish river, before construction of the Lake Washington ship canal in the early 1900s. Lake Washington accumulates relatively large waves from wind blowing over the surface of the lake. The waves are fetch-limited in their height and wave period because the length of the lake is the maximum distance over which the waves can accumulate. Given the spatial and temporal constraints of the lake, the waves tend to have a 'peaky' shape that are closer together and taller than fully developed waves. The strongest waves occur in the winter months, corresponding to the time of year with the highest winds. The lake resource has been characterized by Professor Jim Thomson at the University of Washington Applied Physics Lab. Data collected in the winter of 2012 is used to determine the joint probability distribution of the wave height and peak period of the waves (Figure 9) [45].

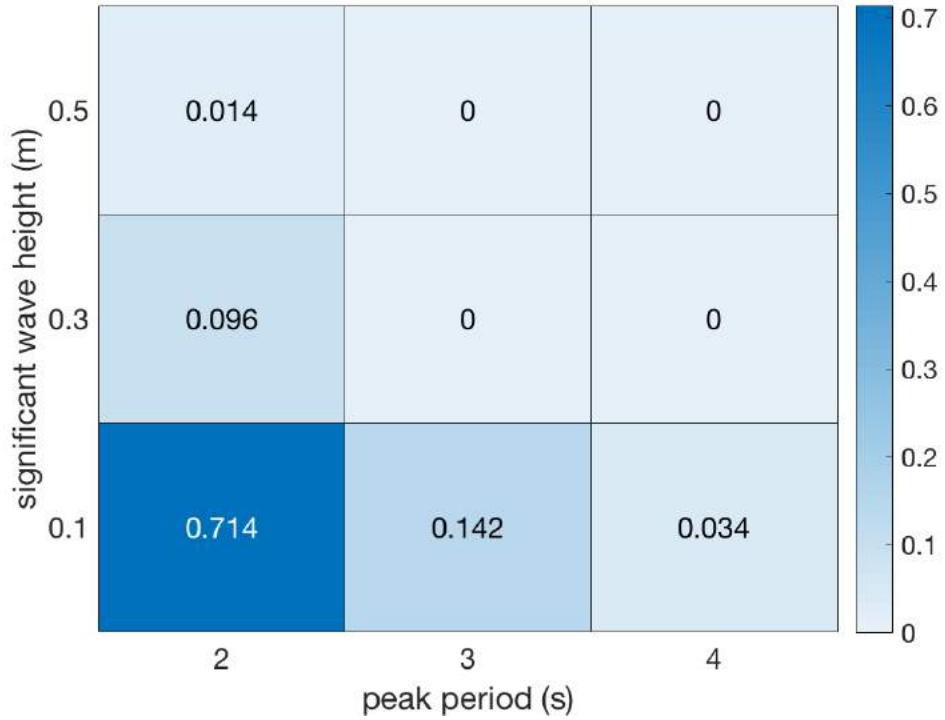

Figure 9 - Joint Probability Distribution Lake WA Winter 2012

A joint probability distribution is used to determine the dominant wave height and wave period combination at a specific wave site. The majority of the Lake Washington wave data collected in the winter of 2012 is in the 1.5 - 4.5 s wave period range and up to 0.6 m wave height. The wave period bins are in increments of 1 s in the range of 1 s to 1.5 s – 4.5 s. The wave height bins are in increments of 0.2 m in the range of 0.01 m – 0.6 m. 85% of the data is within these bins, and the remaining 15% of waves in Lake Washington are described by long-period (25 s), low-amplitude (0.025 m) swell waves. These are not considered in the analysis because they are outside of the operational range of the miniWEC. The five wave bins with 85% of the data are scaled up proportionally to form 100% of the wave resource in the joint probability distribution for the purpose of this analysis.

The energy spectra in Lake Washington can be described by JONSWAP parametric spectra. JONSWAP parametric spectra were developed from wave analysis in the North Sea for waves that were found to always be fetch limited [46]. Fetch-limited waves are peaky and required a peak shape factor to accurately describe them with parametric spectra. In contrast, Bretschneider parametric spectra do not have a peak shape factor and are a better fit for fully developed waves [47].

The 2012 Lake Washington wave data was sampled in 30-minute intervals, with a 1.28 Hz sampling frequency using Datawell Waverider buoys [48]. Data was collected from October 26, 2011 – Jan 11, 2012 and the data analysis included evaluation of the energy spectra from the field measurements [49]. Data from five energy spectra are plotted for the dominant wave case which includes waves that have wave height less than 0.1 m and wave period less than 2 s. The energy spectra are fit visually by plotting idealized JONSWAP energy spectra and Bretschneider energy spectra to estimate the best fit to the idealized spectra. Figure 10 shows the energy spectra data for the dominant wave case of 0.1 m wave height, 2 s period.

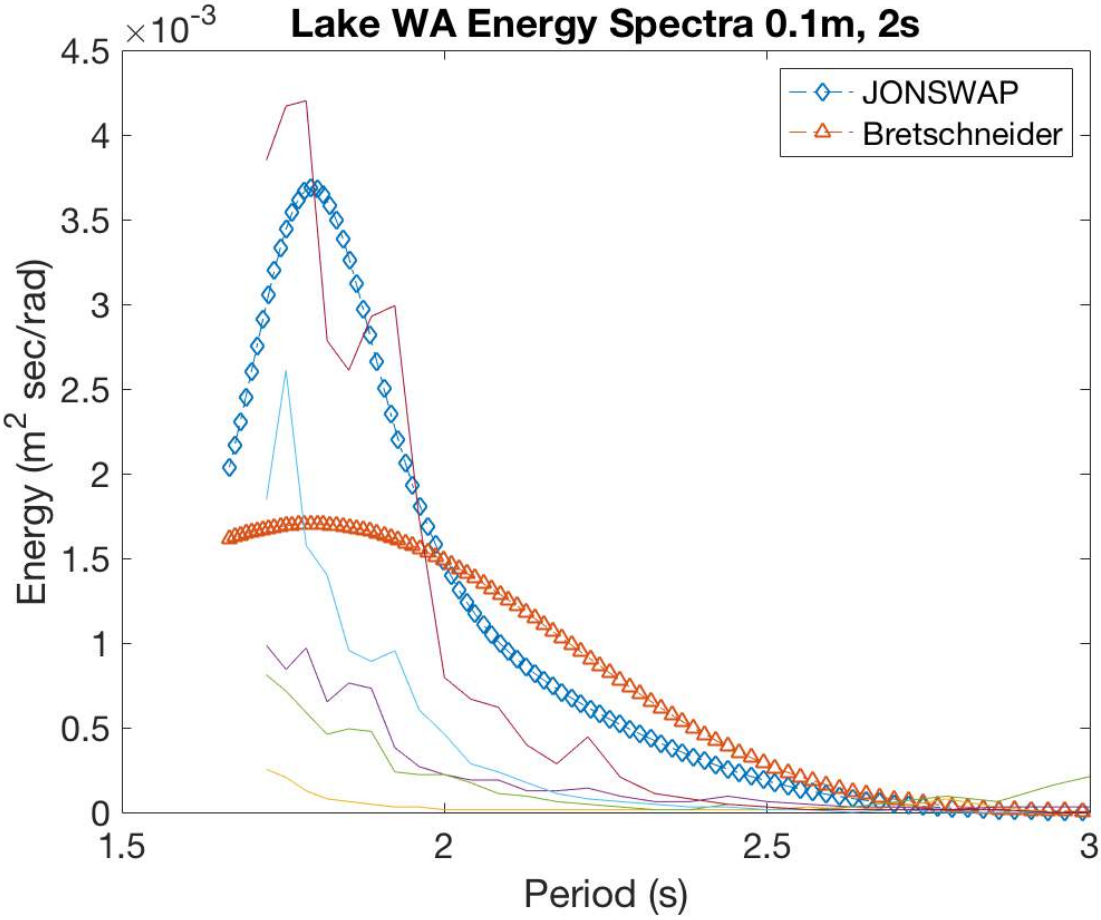

Figure 10 - Energy Spectra Data for Lake Washington Wave Data between 0.05-0.2 m Wave Height and 1-2.5 s Wave Period Compared with JONSWAP and Bretschneider Idealized Spectra

The idealized energy spectra will be used for this analysis, including the peak shape factor, wave height, and wave period for the five wave cases. The idealized spectra are defined by Equation 2.1 with frequency range w, peak frequency w_p, gravity, alpha as defined in Equation 2.2, and the peak shape factor gamma [46-47].

$$S(w) = \frac{\alpha g^2}{w^5} exp\left(-\frac{5}{4}\left(\frac{w_p}{w}\right)^4\right)\gamma^{exp\left(\frac{-(w/w_p)^2}{0.0098}\right)} \quad (2.1)$$

$$\alpha = 5.06 \frac{{H_{m0}}^2}{{T_p}^4} (1 - 0.29 \ln(\gamma)) \quad (2.2)$$

The wave height H_{m0} is defined as four times the standard deviation of the surface elevation and the peak period is T_p. The peak shape factor gamma is 3.3 for JONSWAP energy spectra and the peak shape factor gamma is 1 for Bretschneider energy spectra. The JONSWAP peak shape factor of 3.3 fits well with waves of 0.1 m height and 2 s wave period, because the energy spectra in this range have a peaky shape profile. Additionally, the 0.1 m height waves with 2 s and 3 s period also fit to the JONSWAP energy spectra. The wave cases with larger height of 0.3 m and 0.5 m with 2 s wave period are not has peaky as the low amplitude waves, and appeared to be a better fit with a gamma of 2.5. These are the five wave cases included in the analysis, defined by their height, period, and peak shape factor.

2.1.2 *MiniWEC Wave Energy Converter*

The miniWEC is a two-body point absorber wave energy converter. It was developed by the UW APL to be used as a test platform for wave energy research in Lake Washington. The miniWEC (Figure 11) has a buoyant cylindrical hull and primarily captures energy from vertical, heave motion relative to a submerged heave plate. The device has a power take-off (PTO) system on top of the cylindrical hull. The PTO consists of a tether attached to springs that can freely move relative to the heave plate which is submerged at depth and not shown to scale in the figure. This research study focuses on the cylindrical miniWEC hull.

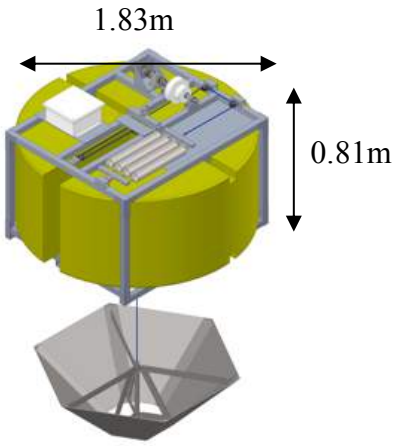

Figure 11 - miniWEC Wave Energy Converter [50]

The cylindrical hull shape of the miniWEC affects its velocity in waves which is directly related to the power output of the system. The hull shape has not been previously optimized for average power or stability and the miniWEC has significant roll and pitch motion in addition to a high center of gravity which may result in the hull flipping over without the heave plate connected. Further, these motions detract from the vertical heave motion and sub-optimal power is achieved. It is thought that significant average power gains can be achieved by optimizing the hull geometry. Through the heuristic optimization method described here, the point absorber hull velocity can be maximized for useful energy production, which could significantly improve the power production and testing capabilities of the miniWEC.

The axisymmetric hull shape is optimized in a defined search space for power development. Axisymmetric point absorbers are non-directional, as they can operate with incoming waves of any incoming direction [6]. The hull geometry search space is defined so that the lower bound is the existing cylindrical miniWEC hull and the upper bound is still able to be deployed with the existing research vessel. The minimum hull shape is set to the existing miniWEC cylinder radius of 0.9 m so that no material will be removed from the existing system. The maximum hull shape

is set to a 1.2 m radius cylinder, which is based on spatial and mass constraints on the R/V Robertson. The candidate hull shapes can vary within the search space, but the submerged volume is kept constant to compare hull geometry with equivalent mass. This is achieved by selecting a baseline cylinder with a radius of 1.1 m and a draft of 0.6 m (a shape between the minimum and maximum radii). Thus, shapes can vary between the minimum and maximum radii and have reasonable drafts, with vertical centroids below the waterline. The candidate hull shapes within the search space are evaluated in the frequency domain using the boundary element method code NEMOH.

2.1.3 *NEMOH Boundary Element Method Code*

NEMOH is an open-source boundary element method (BEM) code which solves first-order wave loading on structures in the frequency domain. BEM is a computational method for solving linear partial differential equations, and NEMOH solves for the added mass, radiation damping, and diffraction forces on offshore structures. Candidate hull shapes are evaluated using NEMOH to solve for their hydrodynamic coefficients. The NEMOH code provides MATLAB scripts to evaluating axisymmetric shapes or 3D hull shapes with custom mesh. There is a MATLAB code for meshing axisymmetric hull shapes based on their shape profiles defined by their radius and draft, and there are 50 sections of the axisymmetric shape about the z axis, and the target number of mesh panels is set at 500. Freshwater density is used and the wave period range of 0.5 - 8 s is considered. The incoming waves are set at 180°, signifying that they are moving towards the hull shape. NEMOH takes approximately 5 mins to evaluate a cylinder and 20 mins to evaluate a shape with several rigid features. The NEMOH hydrodynamic coefficients are smoothed using the MATLAB script ‘medfilt1’ [51] so that any erroneous spikes in the data are removed. The function applies a third-order, one-dimensional median filter assuming no signal beyond the first and last

points. The NEMOH analysis can be used in the genetic algorithm code using MATLAB as the shared platform.

2.1.4 *Genetic Algorithm Toolbox*

A group at the University of Sheffield developed an open-source genetic algorithm toolbox coded in MATLAB [52]. The algorithms in the toolbox are flexible so that they can be used for many applications. A GA uses an objective function to evaluate solutions, and in this case NEMOH can be used within the objective function evaluation to obtain hydrodynamic coefficients which can then be used to imply system power performance within the power proxy. The GA enables an initial population of candidate hull shapes to be generated, which are then evaluated by a user-defined objective function. The set of solutions are ranked, and then highest-evaluating solutions are selected to form the next generation of candidate hull shapes. The GA toolbox provides the scripts that are used for the GA in this research study.

2.1.5 *ProteusDS Time Domain Analysis*

ProteusDS is a time domain software package used for solving wave loading on offshore structures. An existing ProteusDS model of the miniWEC system is used for analysis [53]. The model has been validated in Lake Washington waves and compared to an OrcaFlex model of the miniWEC [54]. The model is used with custom mesh hull shapes in place of the simple cylinder. The five Lake Washington JONSWAP wave cases are run to obtain a power matrix. This model is used as part of the verification of the optimization approach.

2.2 GENETIC ALGORITHM OPTIMIZATION APPROACH

A genetic algorithm is used to optimize the hull shape of a WEC to maximize power development in a specific wave climate. The GA can strategically search within a design space to iteratively improve hull shapes for power output. Development of an accurate proxy for power based on frequency domain analysis is central to this aim. The power proxy becomes the objective function within the genetic algorithm which is used to evaluate and form the basis of ranking candidate hull shapes. The genetic algorithm optimization method is used to identify a high power producing hull shape, which is applied to the axisymmetric miniWEC hull for this evaluation.

2.2.1 *Genetic Algorithm*

The genetic algorithm represents candidate hull shapes as axisymmetric shape profiles. The representation is a 2D profile which represents a slice of the 3D axisymmetric shape, rotated by 360° around the vertical z-axis. The profile shape includes 26 equally spaced vertical points 0.0325 m apart between the top and the base of the 0.81 m hull. Each of the radial points vary between set bounds, and the submerged volume is kept constant by adjusting the draft. Each of the radial points can vary between a minimum radius of 0.91 m and a maximum radius of 1.22 m in increments of 0.01 m, resulting in 32 possible radial positions for each vertical point (Figure 12). The search space is discretized into a grid rather than connecting the points with a spline to allow the GA to identify any shape within the search space. There are 1.4×10^{39} possible profiles within the search space, and an exhaustive search would not be possible at this scale. This problem is well suited to a GA, but the search space is large and would require many iterations to have confidence in shape convergence.

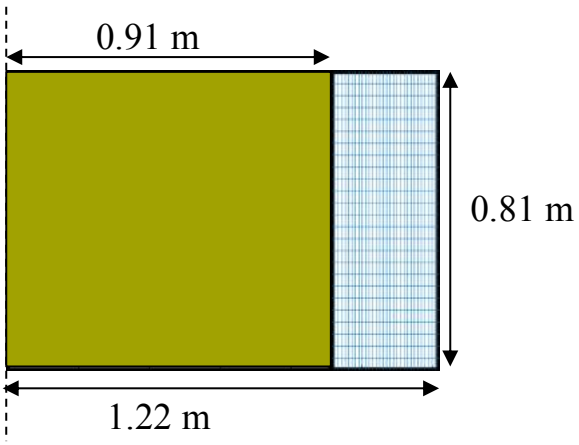

Figure 12 - Axisymmetric miniWEC Shape Profile Search Space

The GA has a population of candidate hull shapes which progress through generations based on an objective function evaluation. The initial population of 30 candidate hull shapes begins with random hull shapes generated by the GA toolbox [55]. The initial population is seeded with three shapes (that will be discussed in the reference shape analysis) to include high power performing shapes in addition to the random shapes. The GA uses a binary representation of the candidate shapes, and there is a precision of 5 used for the 26 points along the shape's edge. Thus, the initial population consists of a matrix that has 30 rows of candidate solutions with 130 columns containing the genetic material. The 30 candidate shape profiles are evaluated by an objective function and ranked based on their result. Figure 13 shows a schematic of the GA process as the initial population of candidate hull shapes are evaluated, ranked, and then enter a generational loop.

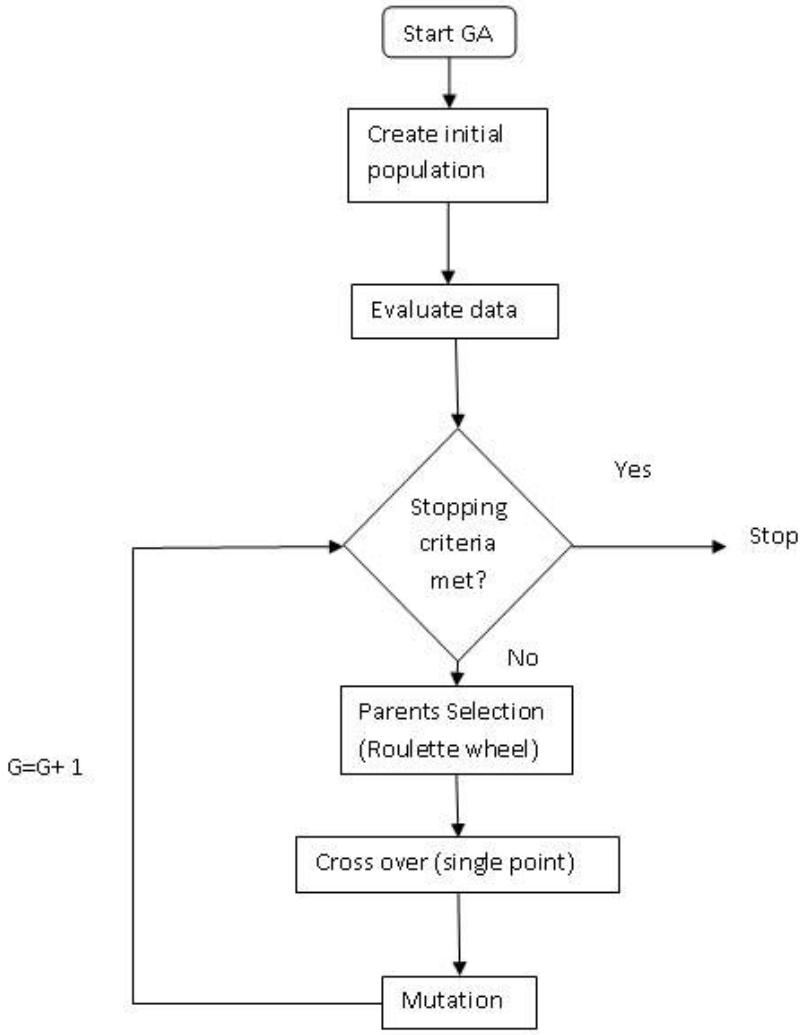

Figure 13 - Genetic Algorithm Process: Initial Population, Evaluation, and Generational Loop [56]

The hull shapes are ranked to select the shapes that will be cloned into the next generation and the shapes that will be used as parents to form offspring. The parents are selected using stochastic universal sampling so that the most fit candidate shapes have the highest likelihood of passing on genetic information. There are 27 offspring created by single point crossover, which are then mutated by 7% to increase genetic diversity. The 27 offspring and 3 clones form the next generation, and this process continues iteratively so that each generation has improved or

equivalent candidate hull shapes as the parent generation. The GA is run for 100 generations, and MATLAB's parallel computing toolbox is used so that multiple candidate hull shapes can be evaluated simultaneously [57]. The GA's ability to identify high power performing hull shapes is dependent upon the objective function evaluation.

2.2.2 *Objective Function*

The objective function evaluates candidate hull shapes within the GA. In this case study, the objective function is the maximization of power. Each shape is meshed and evaluated in NEMOH, and the hydrodynamic coefficients from the NEMOH analysis are used to obtain a proxy for power. The development of this power proxy is presented in the section 2.2.3. The objective function scales the power proxy value to be a non-negative minimization problem, shown in Equation 2.3:

$$Obj\_fun = 5000 - 10(P_{proxy}) \tag{2.3}$$

The GA toolbox ranks the candidate hull shapes based on the minimizing objective function to identify high power producing shapes.

2.2.3 *Development of a Power Proxy*

Central to this work is the development of a proxy for system power that can be calculated through the key components of the WEC response in the frequency domain. The power proxy uses the hydrodynamic coefficients from NEMOH to estimate the power that the new hull shape would produce as part of the miniWEC in the Lake Washington wave climate. While a time domain analysis would be able to give us a direct measure of power produced, it would not be possible to perform this within the GA with our computational resources because it would take too long to

run. Using NEMOH analysis in the GA is computationally efficient compared with using time-domain analysis. However, it is important to have an accurate way to measure power.

The power proxy equation is developed through an analysis of reference shapes. These reference shapes are evaluated in both the frequency domain and the time domain so that the frequency domain power proxy could be compared with the time domain result. The excitation force and 90° optimal phase angle of the hull shapes are being promoted to the next generation. The added mass is also beneficial for power production, but the damping is minimized. These coefficients are integrated over the frequency range and fitted with empirical weights to accurately represent their contribution to power. Additionally, the JONSWAP energy spectrum from the dominant wave case is included in the evaluation to consider enhance the annual energy production of the WEC in Lake Washington. The reference hull shapes that are used as a benchmark to develop the power proxy equation are presented in the evaluation and verification section.

2.3 Reference Hull Shape Analysis

Ten reference shapes are analyzed in the frequency domain and the time domain as a benchmark for comparison, and to form the basis of the power proxy equation. We assessed ten reference hull shapes of equivalent submerged volume (displaced mass) in NEMOH and ProteusDS [25-26]. These results are used primarily to develop the power proxy. Ten hull shapes are selected to be representative of the variation of feasible shapes in the search space. The hull submerged volume is larger than the existing miniWEC hull because the shapes will be added to the existing miniWEC with no material removed. The draft for each shape is calculated using numerical integration to achieve the desired mass of 2,144 kg which is set by the new "baseline cylinder" with radius 1.0668 m and draft 0.6 m. In comparison, the existing hull has 0.9144 m

radius and 0.5286 m draft. The existing miniWEC cylinder and new baseline cylinder are shown in Figure 14 and the remaining nine hull shape profiles are shown in Figure 15.

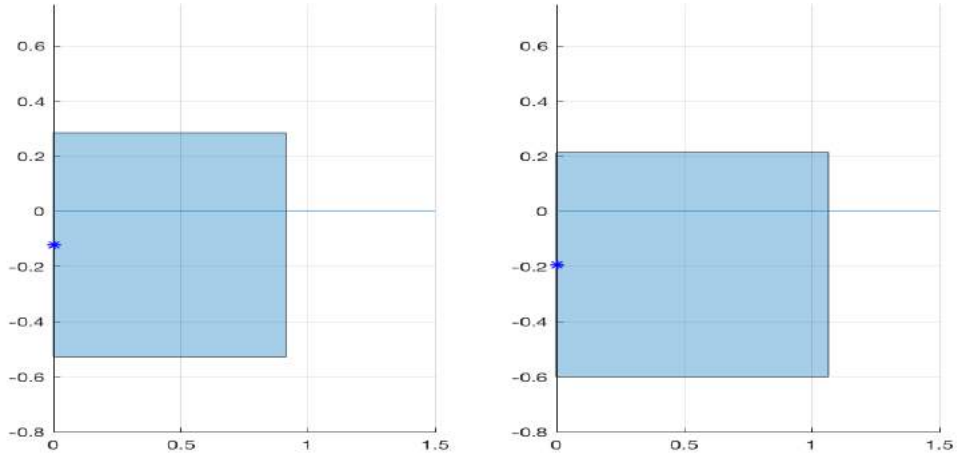

Figure 14 - miniWEC Hull Profile (left) and New Baseline Cylinder (right)

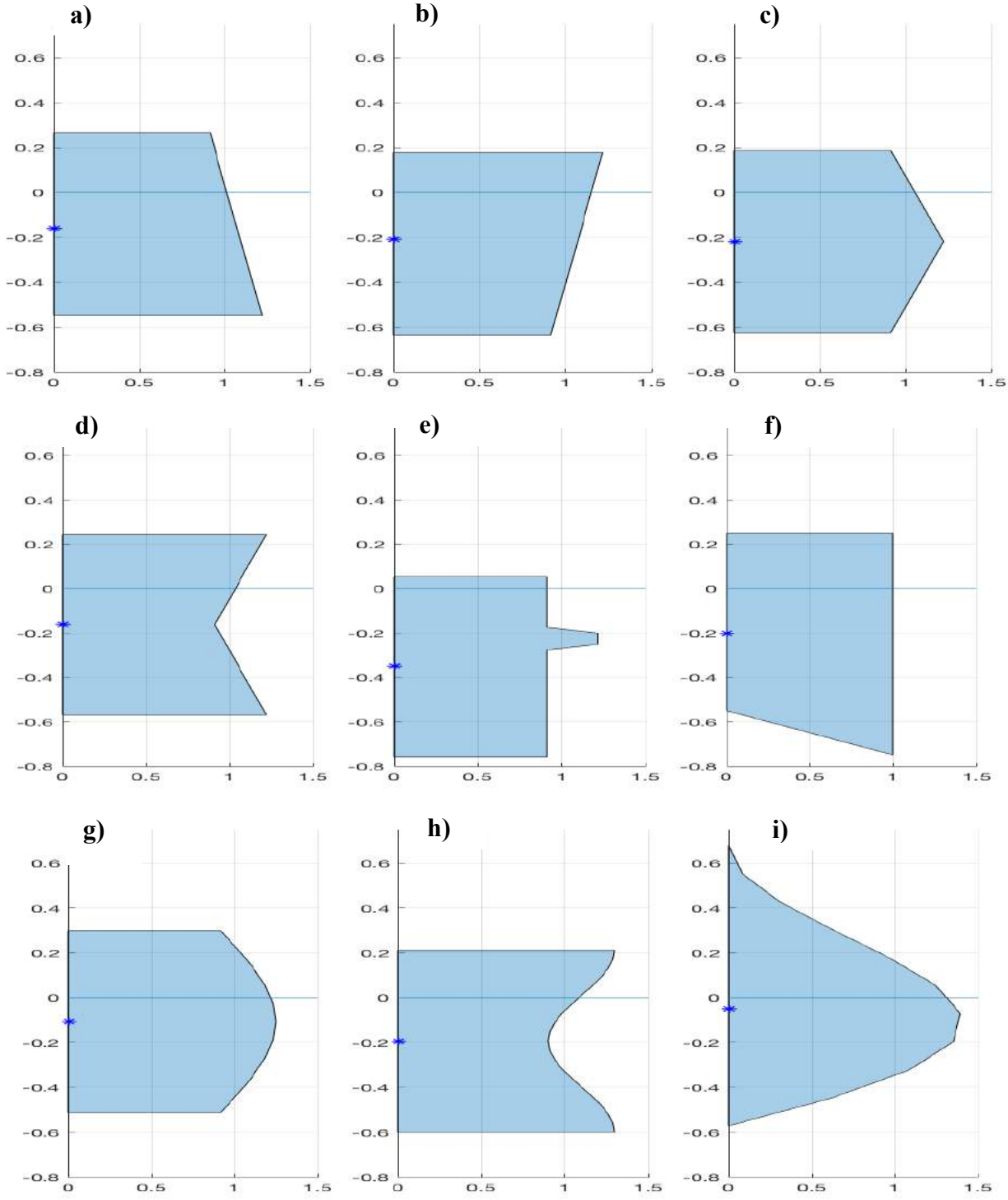

Figure 15 - Reference Shape Profiles for Preliminary Analysis: a) conical, b) reverse conical, c) disk, d) reverse disk, e) fin, f) cavity, g) ellipse, h) hourglass, and i) teardrop

The axisymmetric shapes are evaluated in NEMOH over the 0.5 - 8 s period range and evaluated using the ProteusDS miniWEC model using the five Lake Washington wave cases. Most shapes fit in the search space, but a few extend beyond the search space, and most notably the teardrop shape which has a curved base. The ten reference shapes are evaluated as a benchmark to compare the frequency domain and time domain analysis to form the basis of the power proxy.

2.3.1 *Frequency Domain Analysis of Reference Hull Shapes*

NEMOH calculates the added mass, radiation damping, and excitation forces for the hull shapes. The results presented here describe the vertical heave component. The filtering function 'medfilt1' is used in MATLAB to smooth the NEMOH data throughout the frequency range [51]. The heave added mass (Figure 16), heave radiation damping (Figure 17), and heave excitation force (Figure 18) are shown plotted against wave period for the ten shapes. The heave added mass data is shown for the 0.5 - 8 s period range, and the 1.5 - 4.5 s period range is the primary range of interest as it is dominant in Lake Washington.

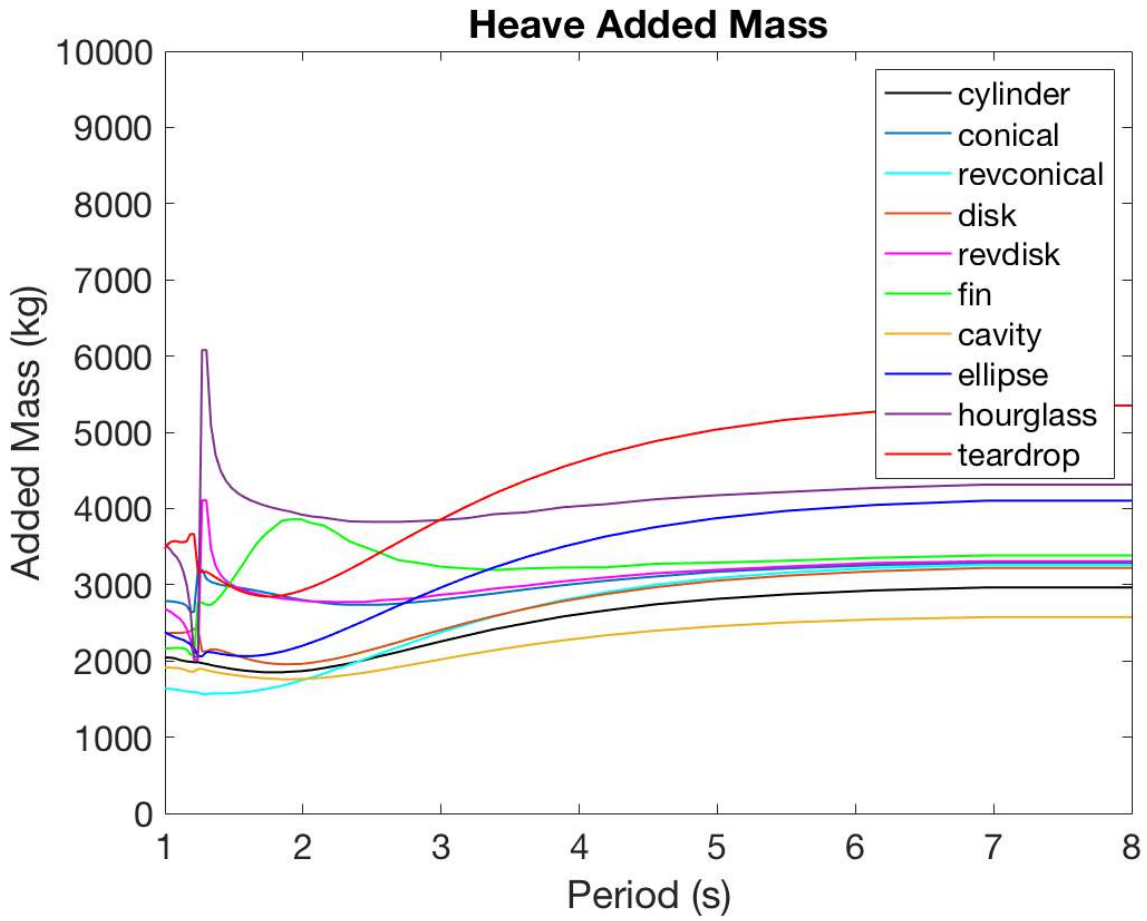

Figure 16 - Heave Added Mass for Ten Reference Shapes

The added mass for the ten shapes varies over the wave period range. The fin shape has the most distinctive added mass plot of the reference shapes. The added mass coefficient of the fin shape peaks around the 2 s wave period, in contrast to the other shapes. The hourglass shape has the largest added mass in the 1.5 - 3 s period range. The teardrop shape has a lower added mass in the 1.5 - 3 s period range, and then has the highest added mass in the largest period range. The heave radiation damping also varies for the ten shapes throughout the wave period range.

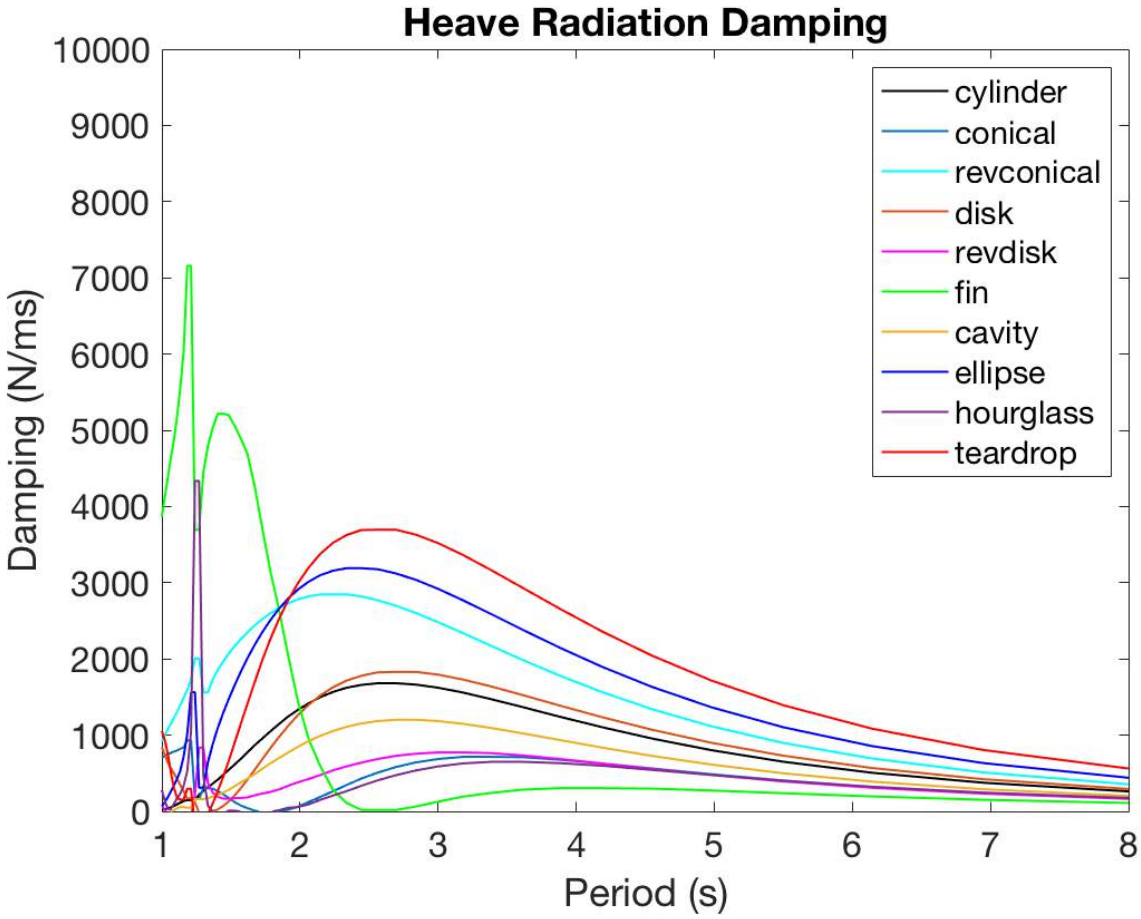

Figure 17 - Heave Radiation Damping for Ten Shapes

The fin shape has the most unique trend in the radiation damping data with a large damping coefficient over the 1 - 2.5 second period range. In contrast, most other tested shapes have an increase in damping between the 1.5 - 3 second period range, which are more gradual and smaller. The teardrop shape has the largest damping coefficient in the 2 - 4 s wave period. The heave excitation force also has unique plots for the ten reference shapes.

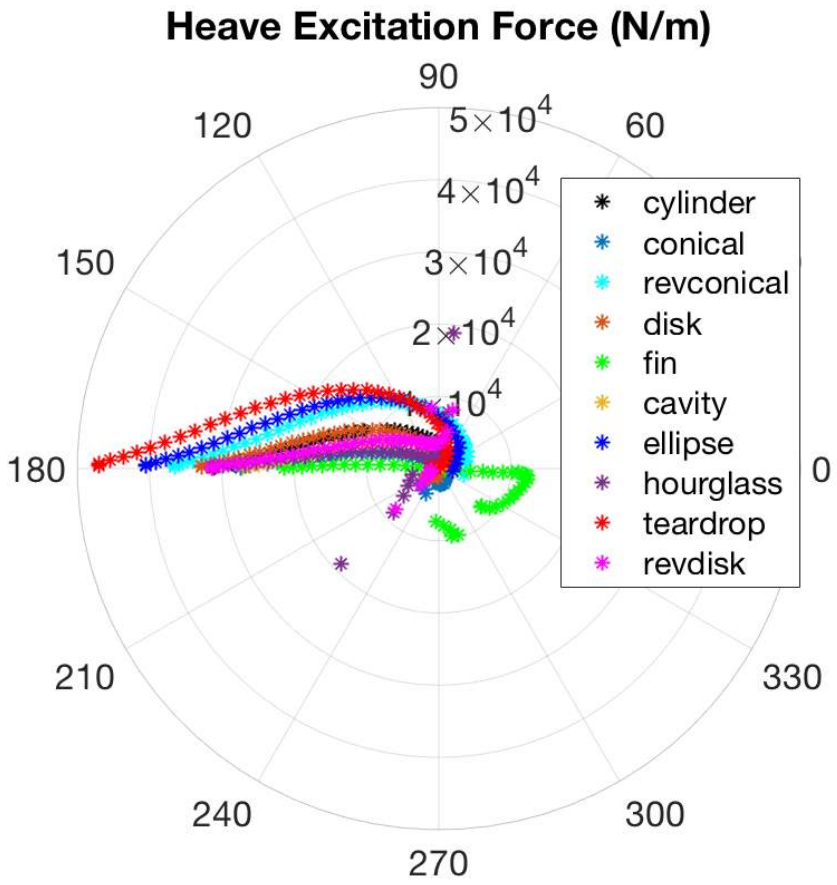

Figure 18 - Heave Excitation Force for Ten Shapes

The heave excitation force is plotted in polar coordinates by the phase angle and excitation force amplitude, which are distinct for the ten reference shapes. The incoming waves approach from 180°, and 90° indicates that the WEC hull shape is in optimal phase with the incoming waves. The smallest wave period is in the center and the largest wave period is to the left of the plot at 180°, with the period range varying between these extremes for 0.5 - 8 s wave period. The fin excitation force shows that the fin excitation is low in amplitude and primarily out of phase with the waves (Figure 18). In contrast, the teardrop, ellipse, and reverse conical shape have a large excitation force amplitude which is significantly in phase with the waves at 90° for a wave period of 0.5 - 3 s. The reverse disk shape is at the 90° optimal phase angle with the waves for a significant

period range of 0.5 - 2 s, and then has lower amplitude in the period range compared to the previous three shapes mentioned. The hydrodynamic coefficients of the ten reference shapes can be compared to the power matrices obtained by time domain analysis.

2.3.2 *Time Domain Analysis of Reference Hull Shapes*

The ten reference hull shapes of equal submerged volume are evaluated in ProteusDS. The power ranking is shown below (Figure 19) referenced from the baseline cylinder of equivalent mass, with the highest to lowest average power producing shape from left to right. The blue portion indicates the cylinder average power, the shapes to the left produce greater power indicated in red, and the shapes to the right produce less power compared to the cylinder indicated in red.

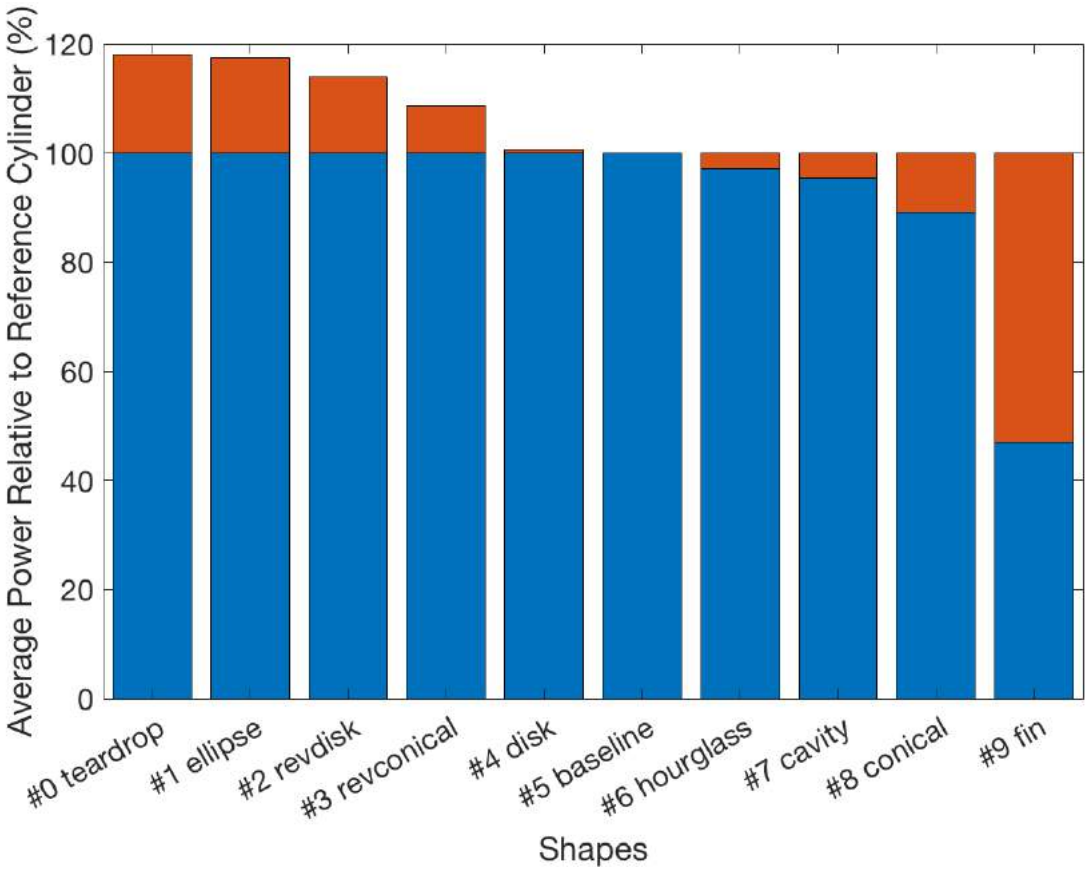

Figure 19 - Average Power of the Ten Hull Shapes Compared with Cylinder

There is significant variation in average power across the ten shapes. The best two shapes, the teardrop and ellipse, have 20% greater average power compared to the baseline cylinder. In contrast, the lowest power performing shape, the fin, has about 50% less average power than the baseline cylinder. These results are used to compare to the results of the frequency domain power proxy equation for the reference shapes.

2.3.3 *Power Proxy Equation*

The frequency domain parameters are empirically weighted to obtain a proxy for the average power of equivalent mass hull shapes. Each of the heave hydrodynamic coefficients are multiplied by the JONSWAP energy spectra for the dominant wave case in Lake Washington. The three coefficients have different units, so the units are standardized to joules. This is achieved by multiplying the radiation damping by the period range and dividing the added mass by the square of the period range. The excitation force term includes the amplitude and the sine of the phase angle. This promotes shapes that are primarily 90° in phase with the incoming waves and large in amplitude. The three terms are then integrated over the frequency range and multiplied by empirically derived weights. Equation 2.4 shows the power proxy equation:

$$P_{PROXY} = a \int \left[M_h S_J \frac{1}{T^2}\right] df + b \int [D_h S_J T] df + c \int \left[Amp(E_h) S_J \sin(\theta_{phase})\right] df \quad (2.4)$$

The weights are determined empirically based on the best fit with the average power for each reference shape evaluated in ProteusDS. The weights are determined to be ‘a’ of 0.4 for the added mass term, ‘b’ of -0.1 for the damping term, and ‘c’ of 0.2 for the excitation force term. It should be noted that although the added mass weight is larger than the excitation force weight, the

excitation force has the greater contribution to the power proxy. The damping term is penalized because shapes with greater damping tended to have less power. Ideally, the hull shapes with the highest excitation force amplitude, 90° in phase with incoming waves, with substantial added mass, and minimal damping will emerge.

The added mass term (Figure 20), damping term (Figure 21), and excitation force term (Figure 22) for the reference shapes are shown prior to integrating over the frequency range and multiplying by the weights. The hourglass shape has the largest added mass contribution, followed by the fin shape and the teardrop shape, while the reverse conical shape has the smallest added mass contribution to the power proxy.

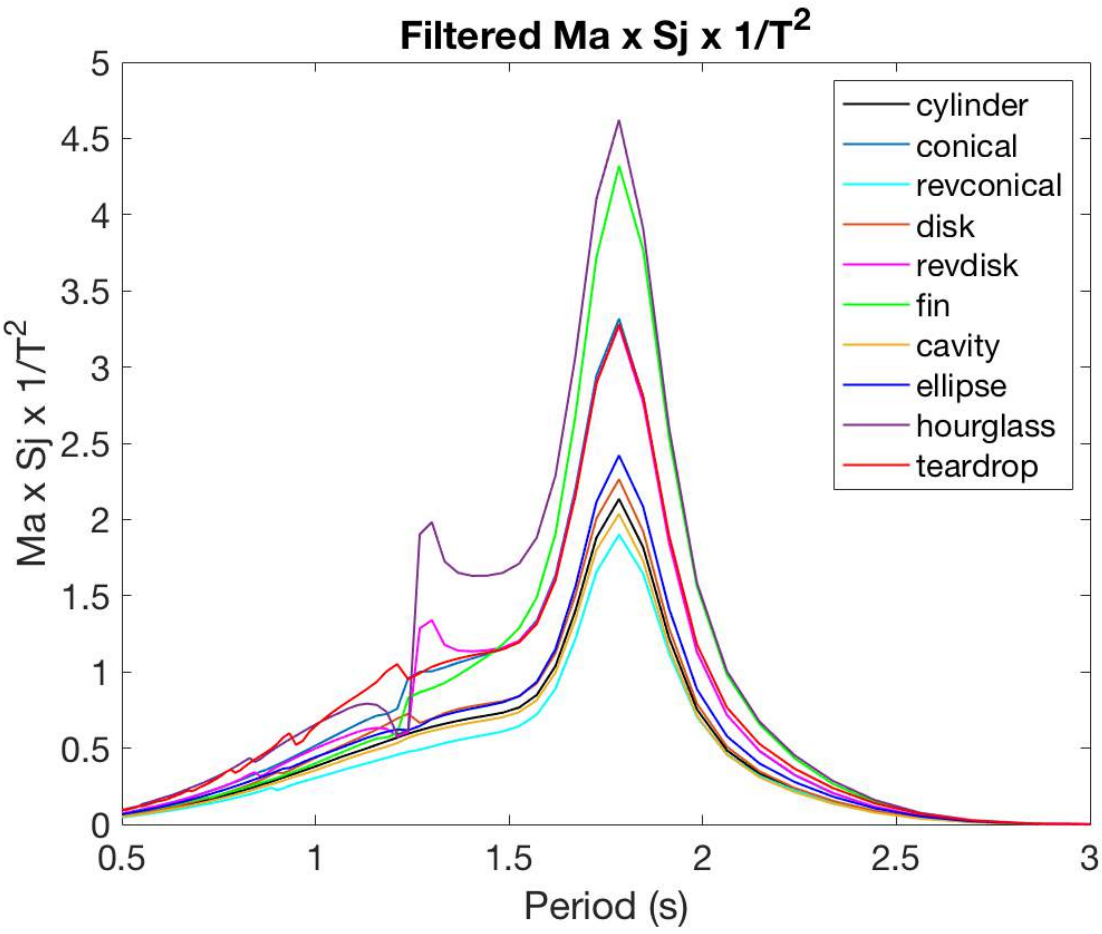

Figure 20 - Added Mass x Energy Spectra x $1/T^2$ [Joules]

The damping term is greatest for the fin shape and smallest for the conical shape. The fin shape has the lowest power production of the reference shapes and also has the highest damping contribution to the power proxy.

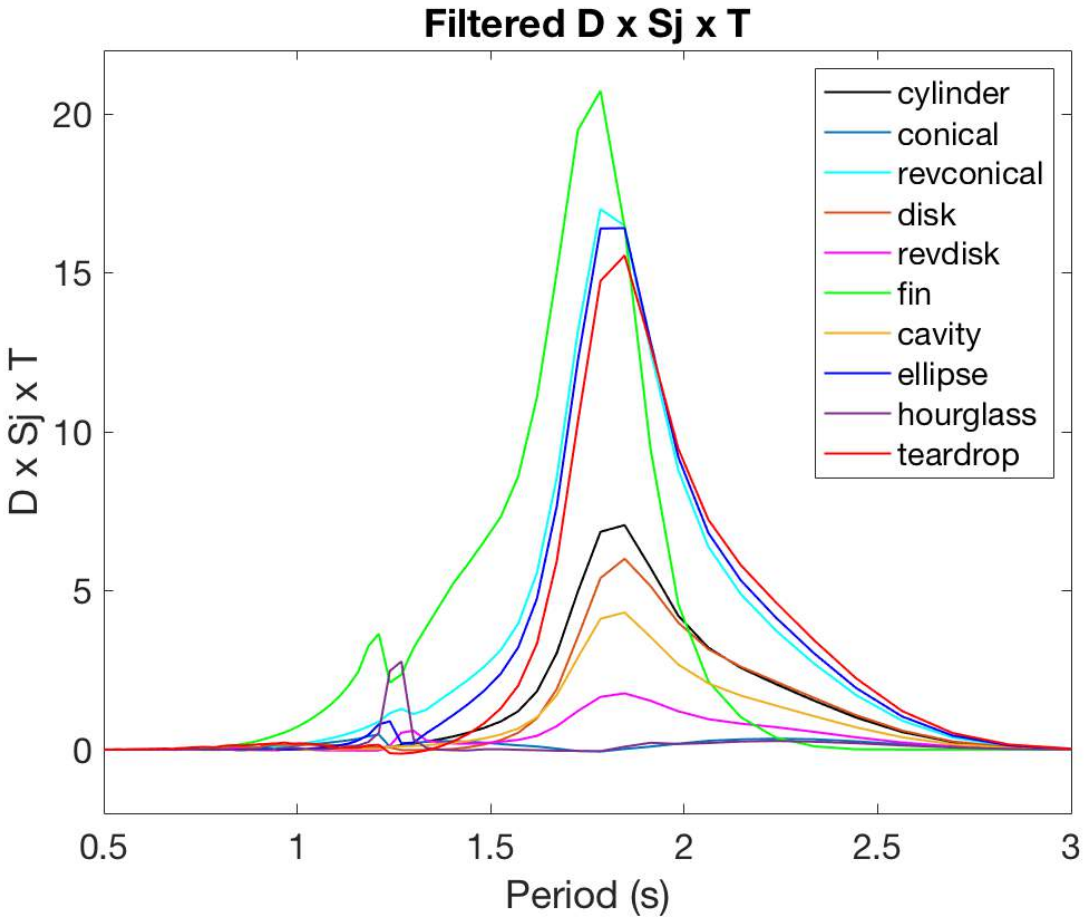

Figure 21 - Damping x Energy Spectra x T [Joules]

The excitation force term is greatest for the teardrop shape and smallest for the fin shape. The excitation force has the greatest impact on power, which matches with the high power performing teardrop shape and low power performing fin shape.

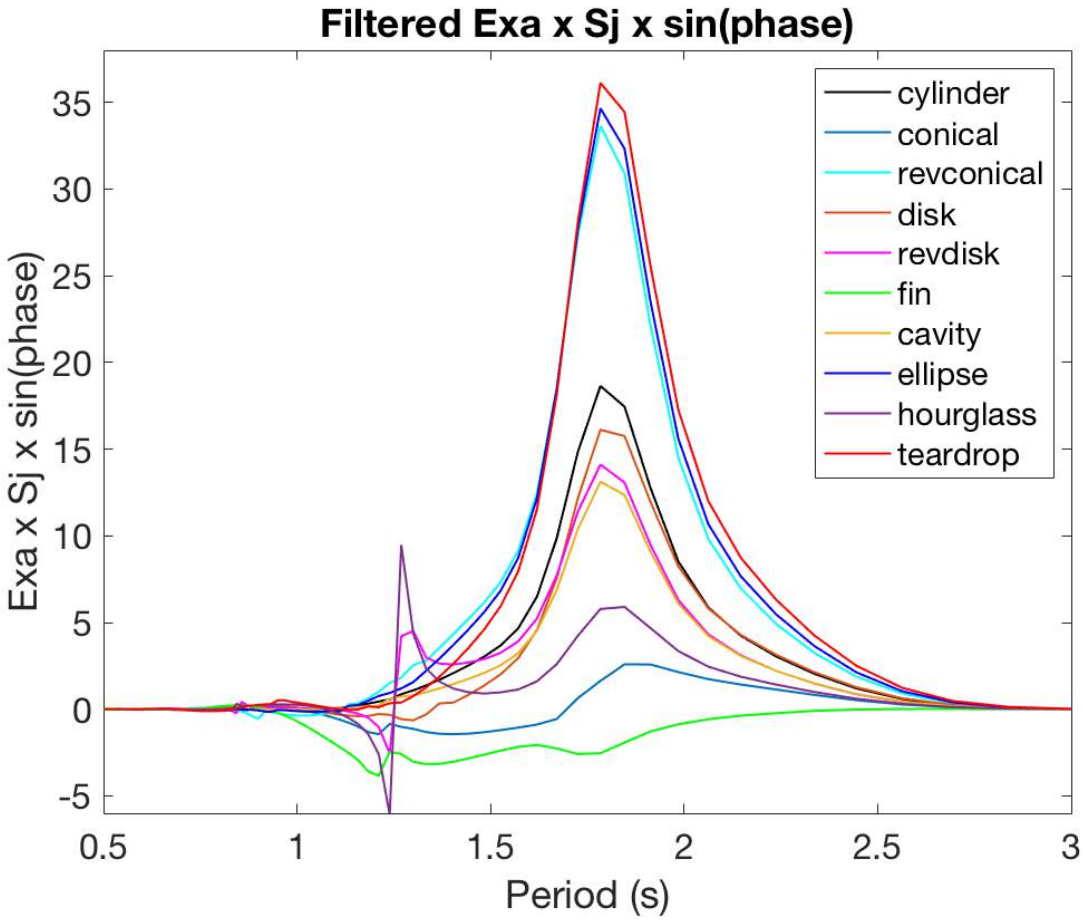

Figure 22 - Excitation Force Amplitude x Energy Spectra x sin (Phase Angle) [Joules]

The power proxy values are compared to the average power from the time domain analysis. The three hydrodynamic components (Figure 20-Figure 22) are integrated over the frequency range, multiplied by the weights, and summed to obtain the power proxy for each hull shape. Overall, the power proxy fits well at around 10% error for half of the shapes. Figure 23 shows the power proxy for each reference shape compared with the ProteusDS average power. The shapes are plotted from the highest power shape on the left to the lowest power performing shape on the right.

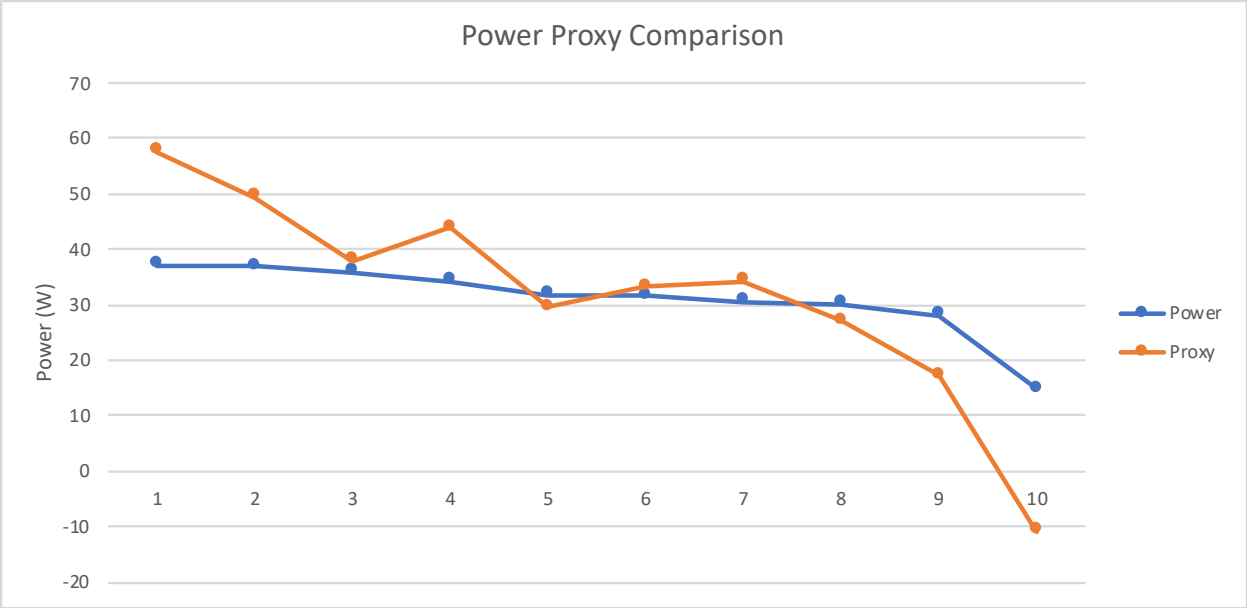

Figure 23 - Power Proxy Comparison

Table 2.1 shows the reference shapes in the same ranking, comparing the average power, the power proxy, the error, and the difference in rank between average power and the power proxy.

Table 2.1. Power Proxy Compared with Average Power Ten Shapes

	Teardrop	Ellipse	Revdisk	Revcon	Disk	Cylinder	Hourglass	Cavity	Cone	Fin
Power (W)	37.2	37.0	35.9	34.3	31.7	31.5	30.6	30.1	28.1	14.8
Proxy (W*)	57.7	49.4	38.0	43.8	29.5	33.2	34.3	27.0	17.1	-10.8
Error	55%	34%	6%	28%	-7%	6%	12%	-10%	-39%	-173%
Rank	1	2	3	4	5	6	7	8	9	10
Proxy Rank	1	2	4	3	7	6	5	8	9	10

The power proxy is able to accurately rank the shapes from highest to lowest power for 7 of the 10 reference shapes. Three of the best shapes are over-predicted and the two lowest power performing shapes are under-predicted. The five remaining shapes are predicted within 6-12% of

the average power from ProteusDS. The power proxy is used within the objective function evaluation of the GA to evaluate power performance of the candidate hull shapes.

2.4 Sensitivity Study of NEMOH Feature Spacing

A sensitivity study is used to understand the sensitivity of NEMOH to shapes with small spacing between features and sharp edges to ensure that the shapes are being accurately evaluated. Shapes with a greater number of horizontal spikes in the hull profile are evaluated, with the points varying between the minimum and maximum radius over smaller vertical increments. The sensitivity of small spacing between features, sharp corners, and shape variation at the waterline are being evaluated. Table 2.2 shows the dimensions of the four shapes with a total of 8, 10, 12, and 14 spikes which have a vertical variation of 0.03 - 0.054 m. The hull shape search space has vertical spacing of 0.0325 m, which would allow a maximum of 13 spikes falling between the final two shapes. Figure 24 shows the shapes plotted from the waterline to the base for the shapes with 8, 10, 12, and 14 total spikes from top to base.

Table 2.2. Sensitivity of Spikey Shapes

Total Teeth	Submerged Teeth	Total Points	Vertical spacing (m)
8	6	16	0.054
10	8	20	0.043
12	9	24	0.035
14	11	28	0.030

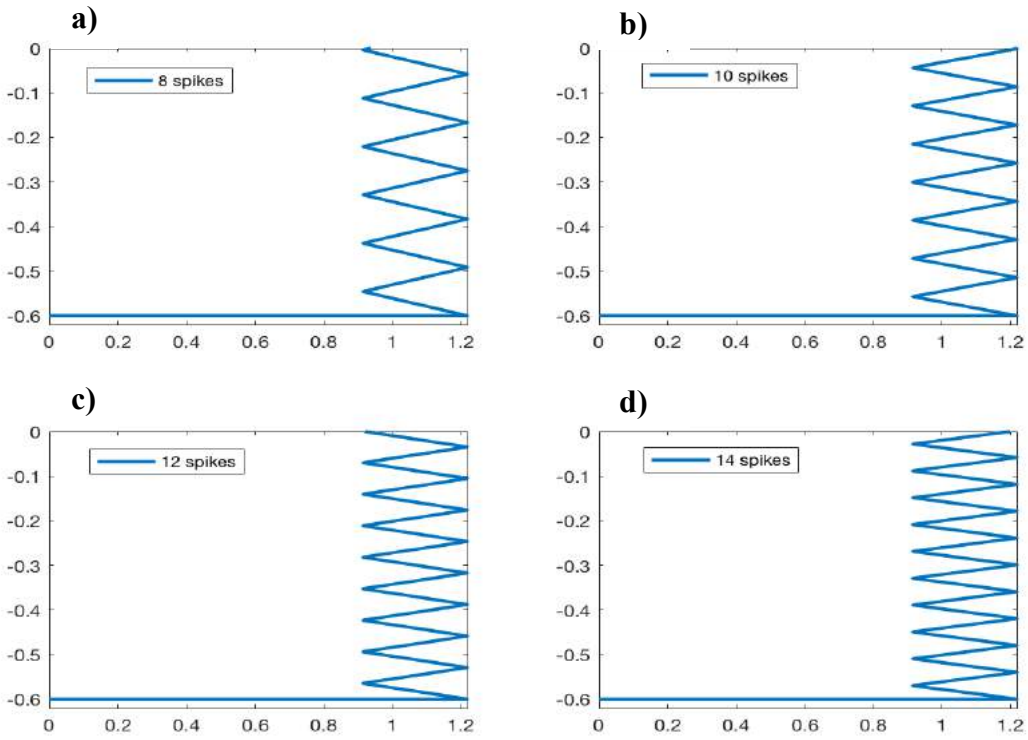

Figure 24 - Shapes Profiles with Greater Number of Spikes: a) 8 spikes, b) 10 spikes, c) 12 spikes, and d) 14 spikes; note waterline maximum radius spike for 10 and 14 spikes compared with waterline minimum radius for 8 and 12 spikes

The study shows that there is a greater sensitivity to the radius at the waterline rather than the vertical spacing between features. Shapes with a maximum radius at the waterline have different results than spikey shapes with a minimum radius at the waterline. The excitation force is plotted in polar coordinates including the phase angle and excitation force amplitude for a 2 s wave period (Figure 25). The wave period of 2 s is used because it is the predominant wave period in Lake Washington. Both the reference cylinder and the maximum radius cylinder excitation force for a 2 s wave period are included in the plot.

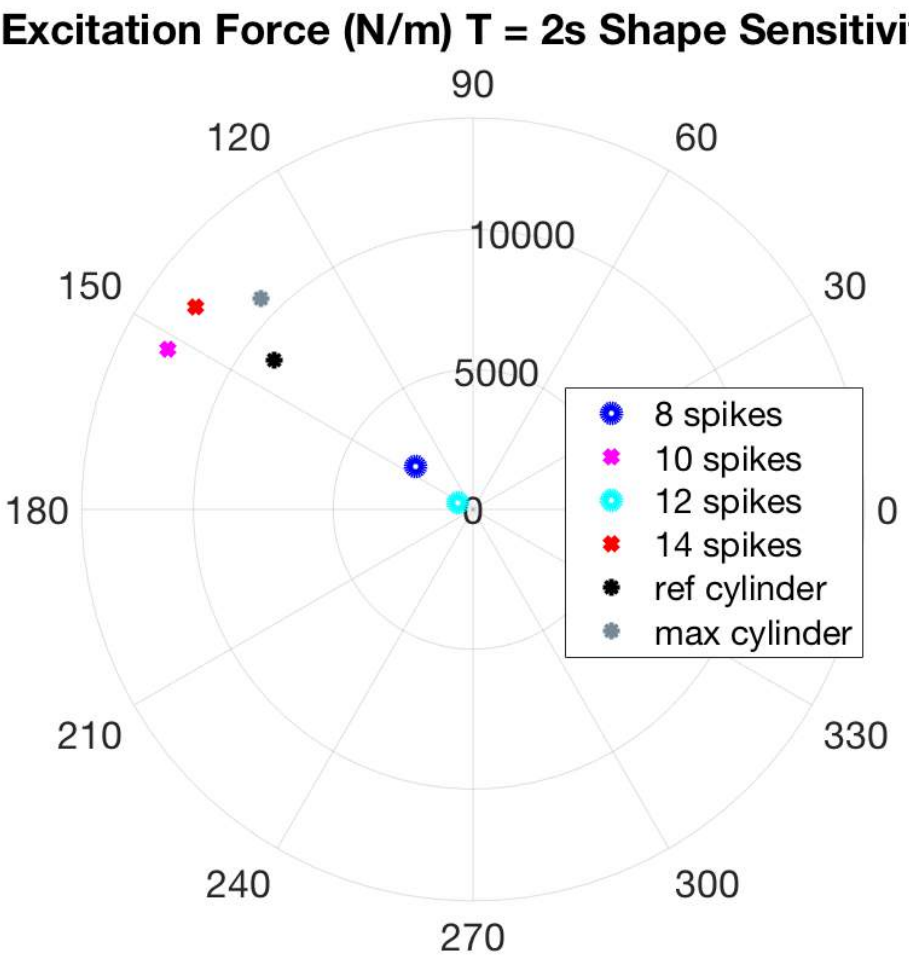

Figure 25 - Heave Excitation Force for the Spikey Shapes at T = 2s Compared with the Maximum Radius Cylinder over the entire period range; note that the 10 and 14 spike shapes have the maximum radius at the waterline, while the 8 and 12 spike shapes have the minimum radius at the waterline

The shapes with 8 spikes and 12 spikes have a minimum radius at the waterline, and both points have low excitation force amplitude. The shapes with 10 and 14 spikes have a maximum radius at the waterline and have a large excitation force amplitude. The excitation amplitude for the 10 and 14 spike shapes is similar to the excitation amplitude for the largest radius cylinder. The reference cylinder has a lower excitation amplitude and similar phase angle. The 8-spike shape has a low excitation amplitude, and the 12-spike shape has an excitation amplitude near zero. The

reference shapes include shapes with the minimum radius at the waterline and the maximum radius at the waterline, which result in a range of average power values for the various hull shapes.

2.5 TIME DOMAIN EVALUATION

The ProteusDS miniWEC model [53] is used to evaluate hull shapes in the Lake Washington wave climate. The model is used for the reference shape evaluation and also to evaluate hull shapes identified by the GA. Each hull shape is meshed using the CAD software Rhino to create a GDF mesh to input in the model [58]. The five JONSWAP wave cases are each evaluated using 20 s of ramp time for the waves to develop and a total of 200 s of run time. The five wave cases are described by their wave period, wave height, and peak shape factor which are shown in Table 2.3. The same random waves are used for every hull shape evaluated.

Table 2.3. Lake Washington JONSWAP Wave Cases

Significant Wave Height (m)	Peak Period (s)	Peak Shape Factor
0.1	2	3.3
0.3	2	2.5
0.5	2	2.5
0.1	3	3.3
0.1	4	3.3

The model includes linear hydrodynamic coefficients from NEMOH, nonlinear forces on the hull, a submerged heave plate, and a linear prismatic power take-off system. The NEMOH data for each hull shape is input as hydrodynamic coefficients. Additionally, the custom mesh is used to calculate nonlinear hydrostatic stiffness and Froude-Krylov forces. The power take-off (PTO) system is modeled as a prismatic linear joint with a damping rate of 300 Ns/m. There is linear quadratic drag added to the base of each hull, using 100 Ns^2/rad^2 for the yaw component. The

model also includes the heave plate and tether connection between the two bodies. The results from each ProteusDS model run can be output to MATLAB for evaluation.

A power matrix can be created for each hull shape by estimating the average power for each of the five wave cases. The power is estimated using the PTO velocity over time using Equation 2.4.

$$Power = \int_{20}^{200} \frac{cV}{\Delta t} \quad (2.5)$$

The damping rate c is 300 Ns/m, the time interval is 180 s, and the velocity is integrated over this time range. The average power is evaluated for an individual hull shape for each of the five wave cases. The time domain model is used to evaluate the final shape identified by the GA.

Chapter 3. RESULTS

The GA is used to identify high power performing hull shapes for the miniWEC in the Lake Washington wave climate. The methods could be applied to other studies, and these results show improvement for this specific application. The objective function is used to identify high power performing shapes within the GA. The GA is run for 100 generations, and the resulting hull shape in addition to the best shape at 50 generations are evaluated in the frequency domain and the time domain. The GA identifies hull shapes for this specific evaluation case.

3.1 GA Hull Shapes at 100 Generations and 50 Generations

The genetic algorithm improves the power performance of the miniWEC hull in Lake WA conditions after 100 generations of 30 individuals. The final shape at 100 generations is presented in addition to an intermediate shape at 50 generations. The shape at 50 generations produces

substantially more power than the existing miniWEC hull and the shape at 100 generations produces more power still. The final hull shape produces three times the average power of the existing miniWEC as evaluated by the miniWEC ProteusDS model. Figure 26 shows the final hull shape identified after 100 generations (right) and the best hull shape at 50 generations (left).

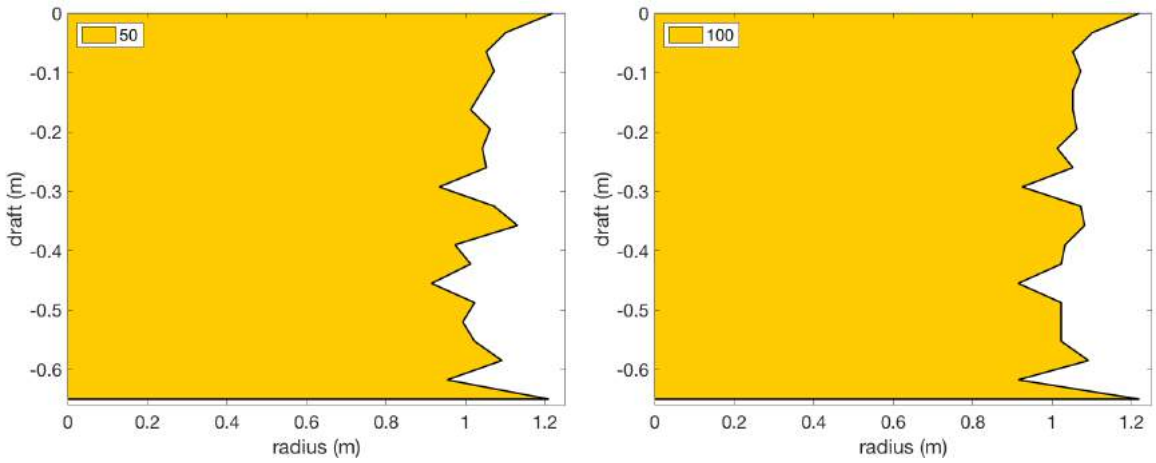

Figure 26 – Generated Shape Profiles 50 Generations, (left), 100 Generations (right)

The GA quickly (over 20 generations) moves towards a shape with the largest radius at the waterline and base, with some other features between including three small fins with jagged profiles. The 100-generation shape is similar to the 50-generation shape, but with more smoothing of the features from the waterline to the base. The 100-generation shape has a power proxy value of 67 W* and the 50-generation hull shape has a power proxy value of 64 W*. The units of 'W*' are used to indicate a proxy power unit. The proxy power performance for the best hull shape at each generation over 100 generations is shown in Figure 27.

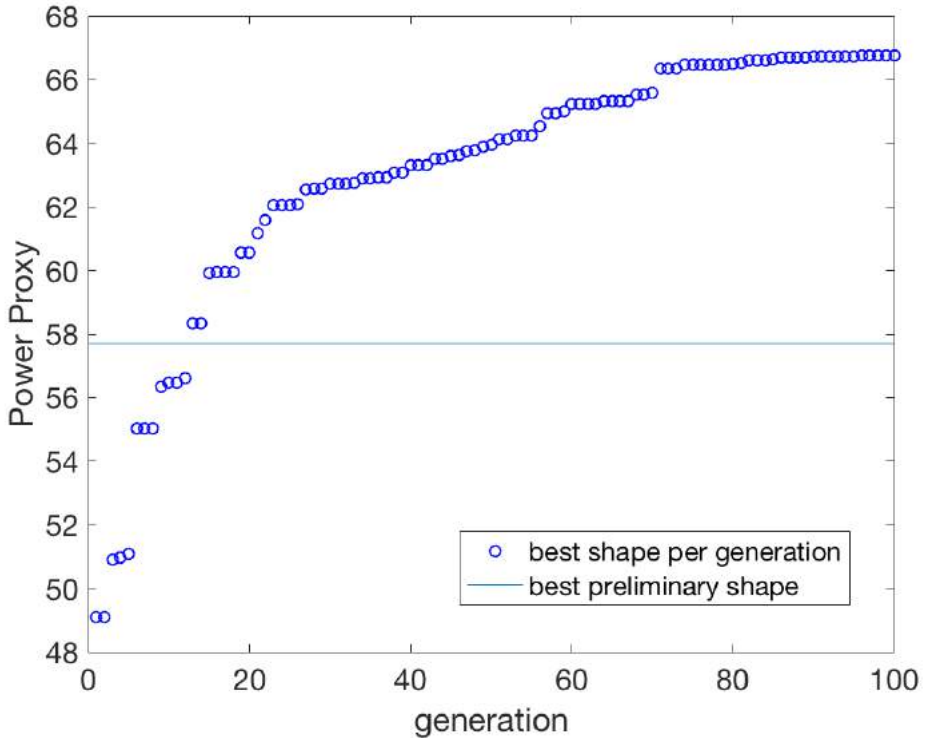

Figure 27 - Best Shape Proxy over 100 Generations

The power proxy for the best hull shape after each generation is shown. The power proxy is improved upon or remains the same as the previous generation as the GA progresses, with more incremental improvements around 25 generations and again around 70 generations. The teardrop reference shape proxy is plotted as a horizontal line to compare to the best shape at each generation. The teardrop shape is outside the design search space and is not one of the reference shapes seeded in the initial population, but is the highest performing reference shape shown for comparison. The power proxy of the best shape within the GA exceeds that of the teardrop shape after 13 generations, and the 100-generation hull shape produces 40% more power than the teardrop shape.

3.2 Frequency Domain Analysis of GA Shapes

The frequency domain results are shown for the 100-generation shape compared to a straight sided cylinder that has the same mass and waterline, the baseline cylinder. The power proxy added mass, damping, and excitation force terms are shown prior to integrating, weighting, and summing the terms to visualize the difference between the optimized shape and the cylinder. The added mass terms for the 100-generation hull shape and the baseline cylinder are plotted against wave period (Figure 28).

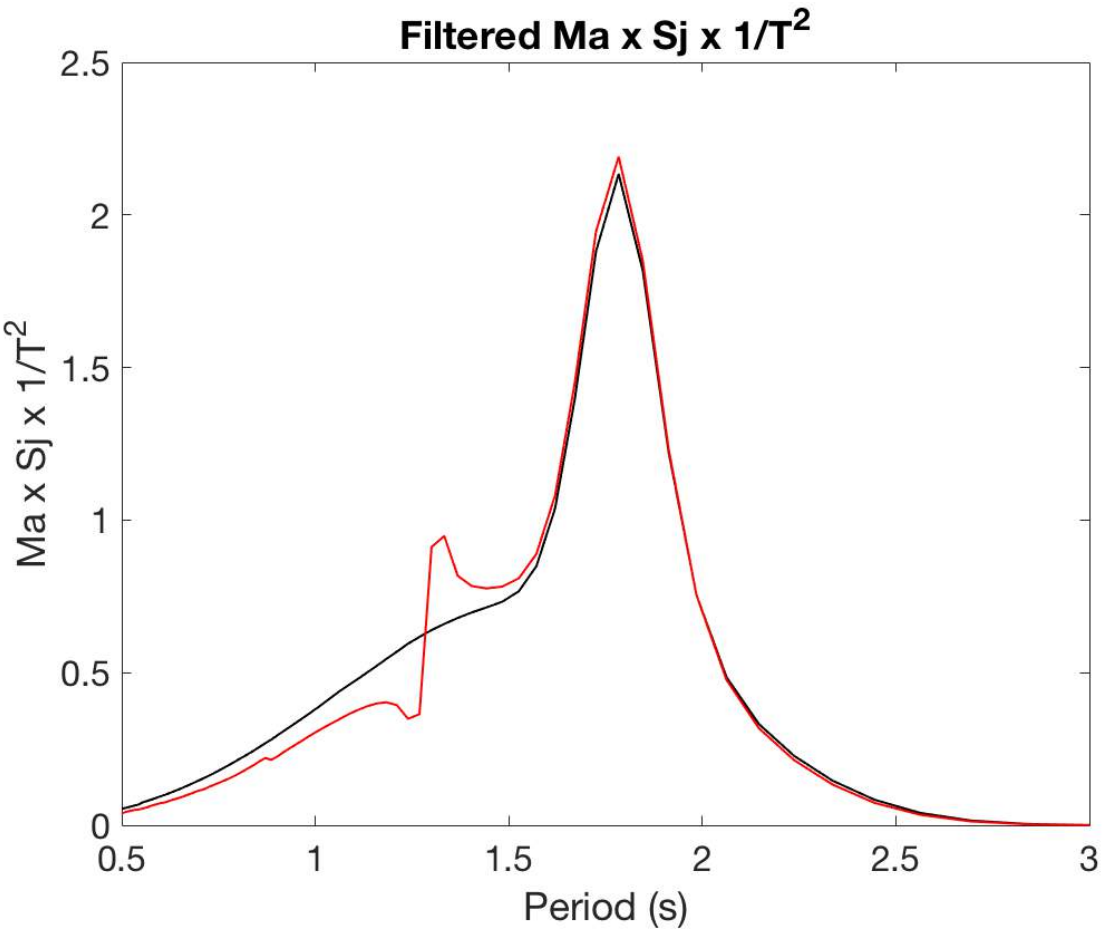

Figure 28 - Added Mass Proxy before Integration - Best Shape and Cylinder

The added mass term for the optimized hull shape is very similar to the added mass term for the cylinder, with the main difference being the increase in 100-generation hull shape plot at 1.3

second wave period. In contrast to added mass, the damping term has a much more distinct variation between the final shape and the baseline cylinder (Figure 29).

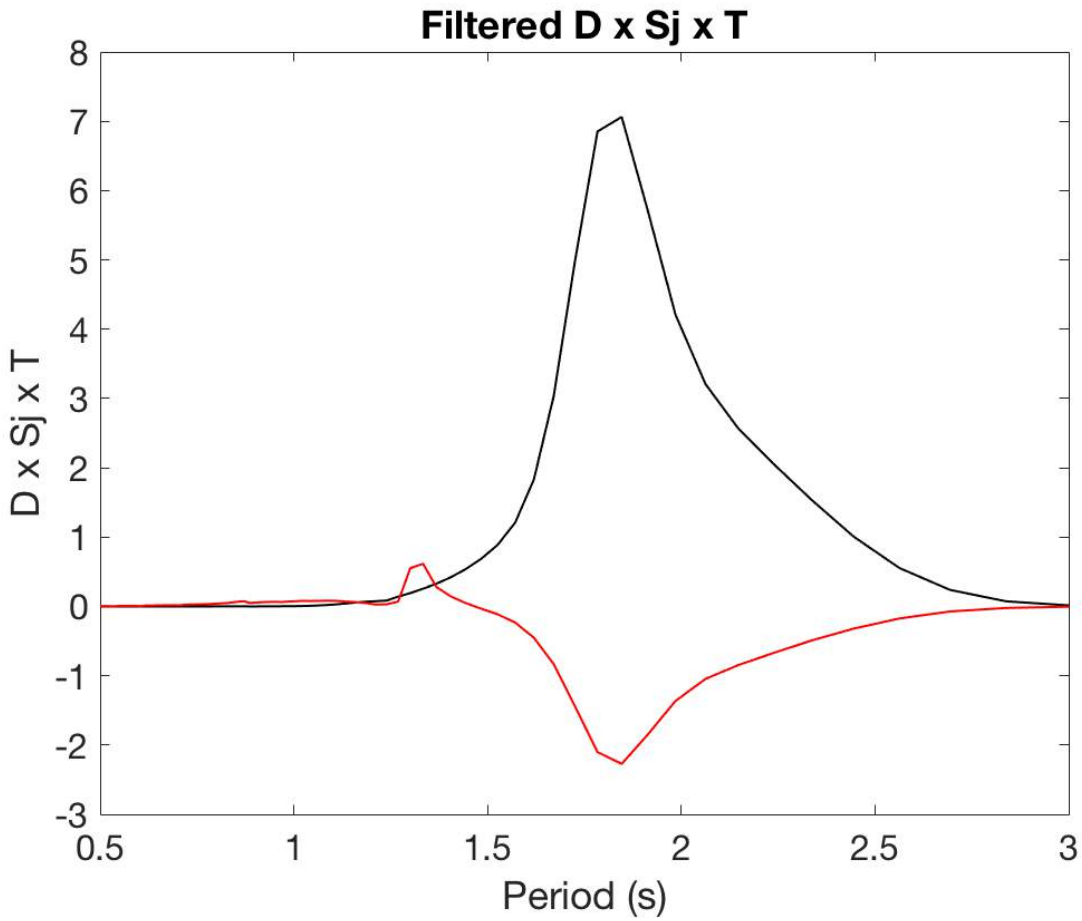

Figure 29 - Damping Proxy before Integration - Best Shape and Cylinder

The radiation damping proxy term for the 100-generation hull shape is negative over most of the period range. In contrast, the cylinder has a positive damping term. Finally, the excitation force proxy term for the 100-generation shape is significantly larger than for the cylinder (Figure 30).

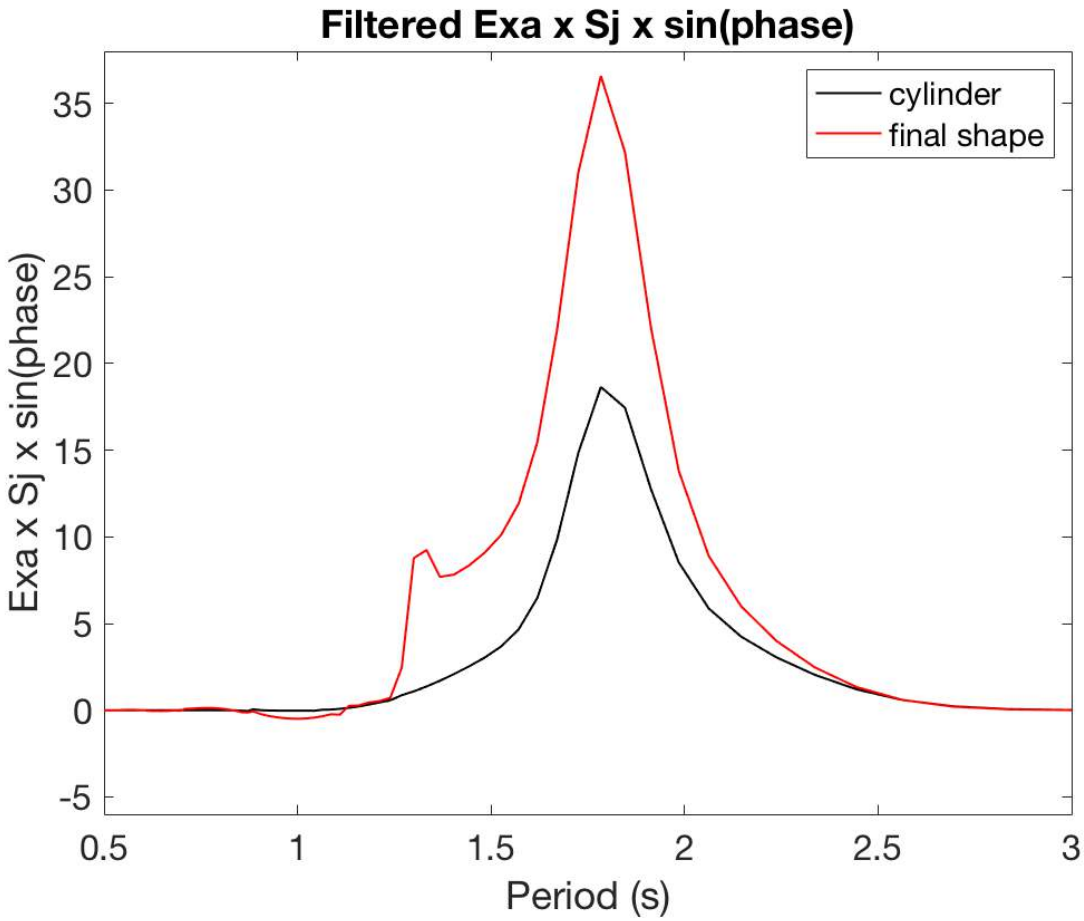

Figure 30 - Excitation Force Proxy before Integration - Best Shape and Cylinder

The final hull shape excitation force proxy term increases rapidly for the 1.3 s wave period and reaches a maximum around 1.75 s wave period. All three power proxy terms for the 100-generation shape have a feature at the 1.3 s wave period, while the cylinder does not have this feature. The hydrodynamic coefficients for the 100-generation shape and the cylinder are shown plotted against wave period (Figure 31-Figure 33). Figure 31 shows the heave added mass for the 100-generation hull shape and the baseline cylinder.

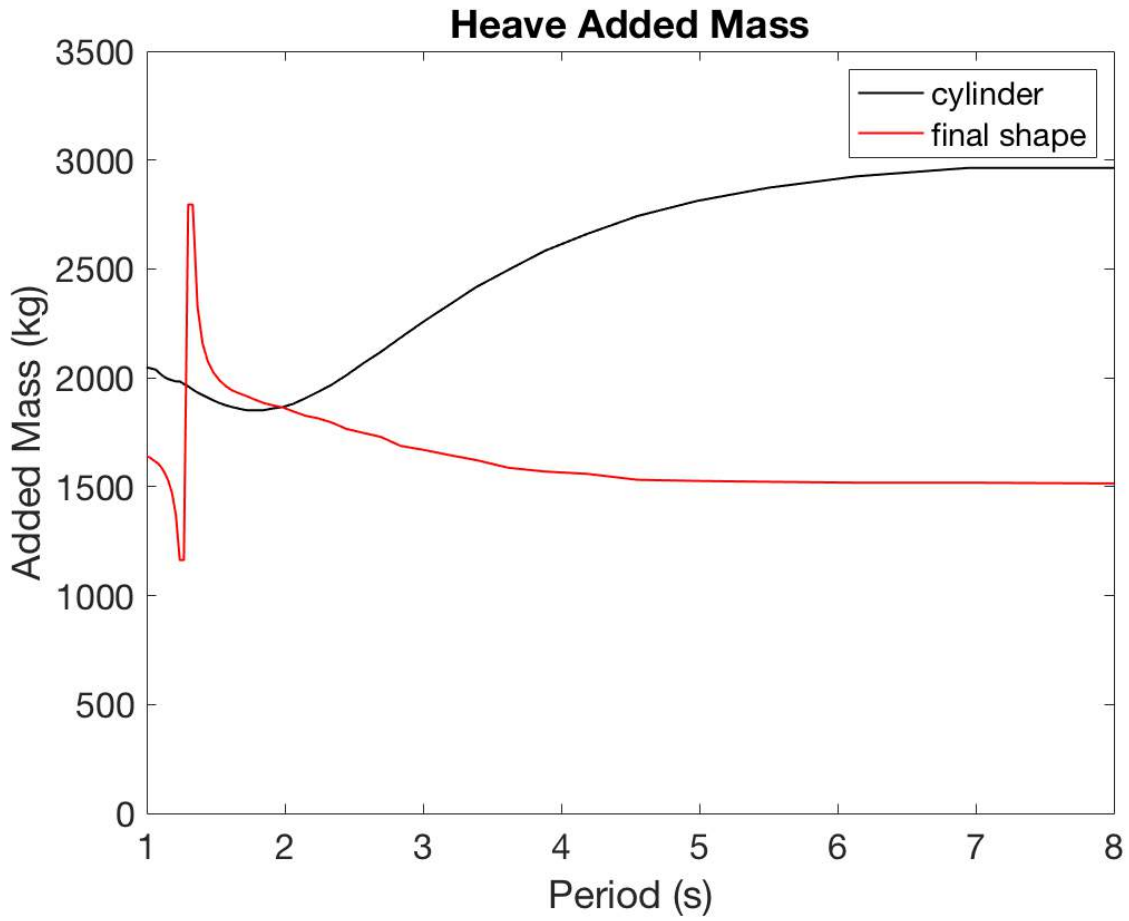

Figure 31 - Added Mass Comparison - Final Hull Shape and Cylinder

The 100-generation hull shape has a heave added mass has a spike increase around 1.3 s wave period to around 2,800 kg, and then the added mass decreases for larger period waves. In contrast, the cylinder begins with a low added mass in the 1-2 s range, and then increases with greater wave period. The heave radiation damping for the 100-generation shape and the cylinder are also distinctive (Figure 32).

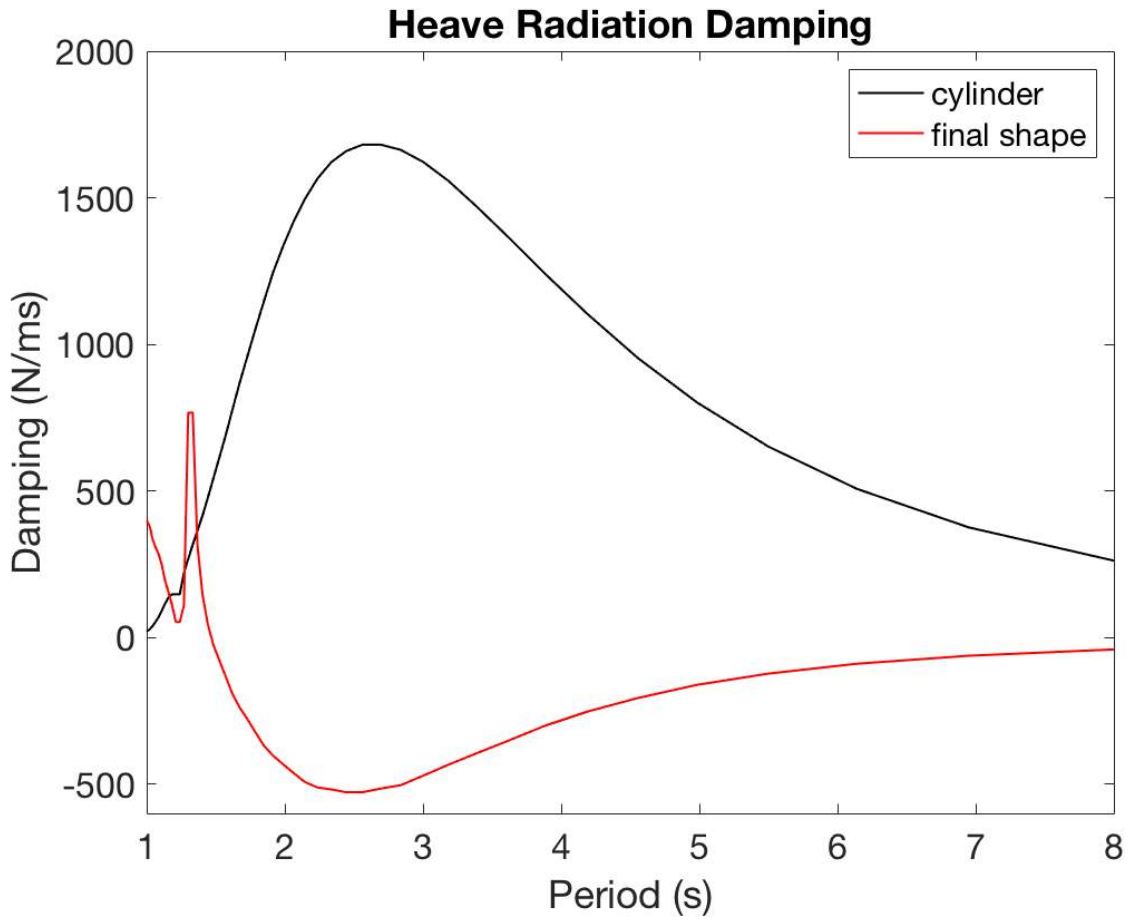

Figure 32 - Damping Comparison - Final Hull Shape and Cylinder

The 100-generation hull shape has a spike around 1.3 s to 750 Ns/m, and then has a negative radiation damping coefficient for most of the wave period range up to -500 Ns/m. In contrast, the reference cylinder increases in damping to around 1700 Ns/m for the 3 s wave period. Finally, the heave excitation force plot for the 100-generation shape is significantly different than for the baseline cylinder (Figure 33).

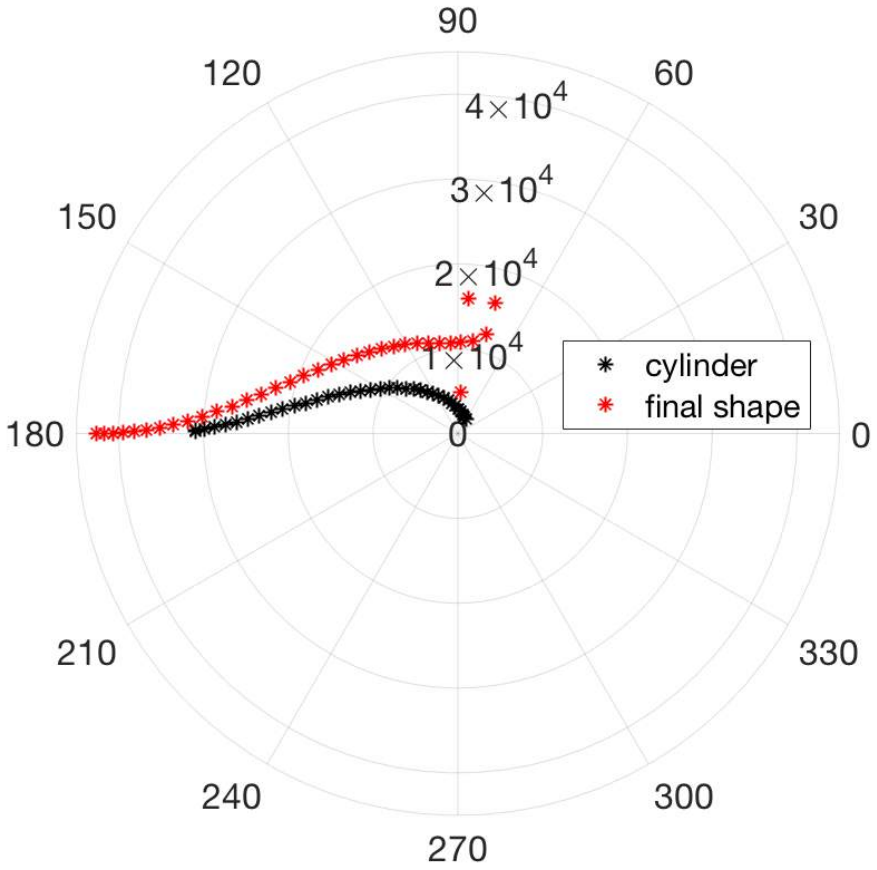

Figure 33 - Excitation Force Comparison (N/m) - Final Hull Shape and Cylinder

The 100-generation hull shape has a large excitation force amplitude and is at near the 90° optimal phase angle for the 1.25-4.5 s wave period which is predominant in Lake Washington. In particular, for the low wave period range of 1.25-2 s the excitation force amplitude is $1x10^4$ N/m and 90°, while the cylinder is near zero in this same range. The 90° phase angle with the waves is optimal, and it is ideal to have the optimal phase angle over a wide range of wave period. The final hull shape hydrodynamic coefficients are optimized in the wave period range corresponding to the Lake Washington energy spectra of 1.5-4.5 s, and especially in the dominant 2 s wave period. The frequency domain hydrodynamic coefficients are input into the non-linear time domain model to obtain a power proxy for the 100-generation hull shape.

3.3 Time Domain Analysis of GA Shapes

The 100-generation hull shape and the 50-generation hull shape are both evaluated with the ProteusDS time domain model to estimate their power output. For comparison, the baseline cylinder with equivalent submerged volume has an average power of 32 W, and the existing miniWEC has an average power of 20 W. The 50-generation hull shape produces an average power of 52 W as part of the miniWEC operating in Lake Washington, which is a power gain of 1.64 compared to the baseline cylinder and 2.6 times compared with the existing miniWEC. The proxy predicted the shape would produce 64 W*, over-predicting by 24%. Figure 34 shows the power matrix for the 50-generation hull shape.

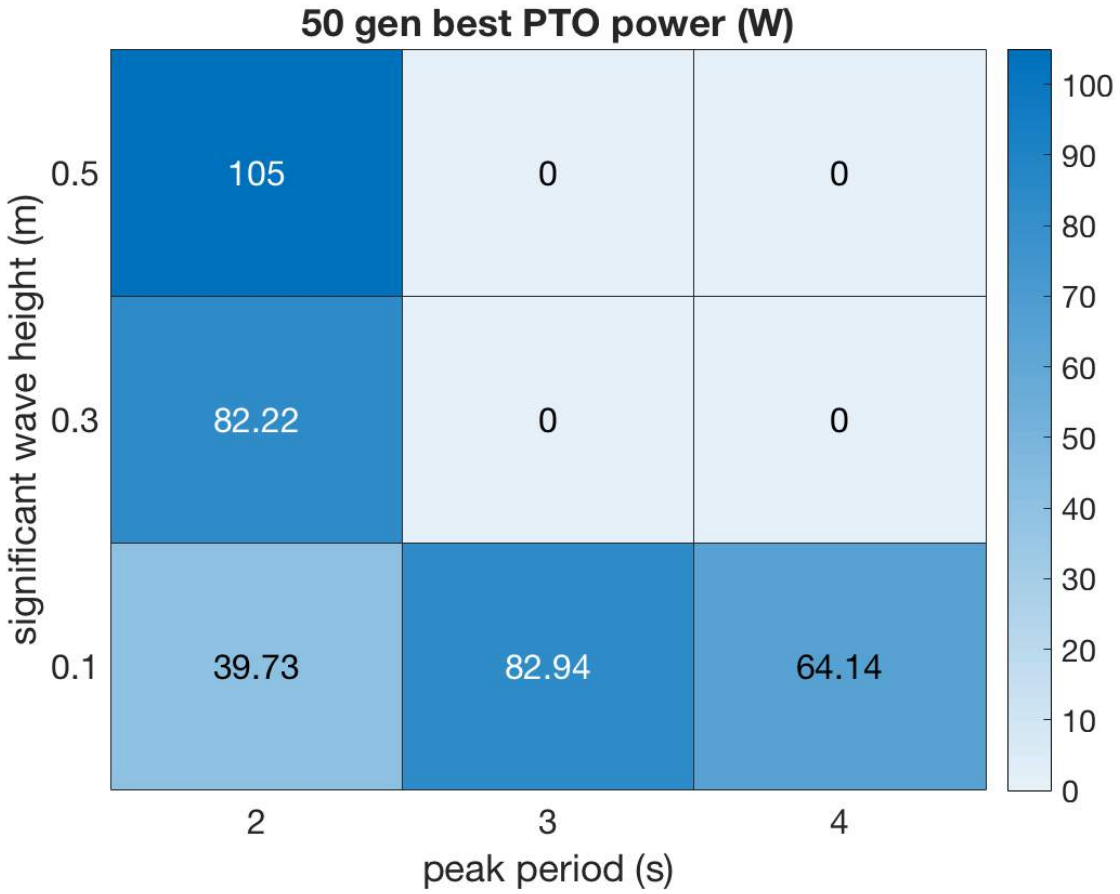

Figure 34 - 50-Generation Shape Power Matrix

The peak power is predicted to be 105 W for the 0.5 m wave height case. Additionally, the greatest power gains occur in the dominant wave case of 0.1 m height, 2 s wave period. The 100-generation hull shape is also evaluated in the ProteusDS model, with the hull shape shown in the model below (Figure 35).

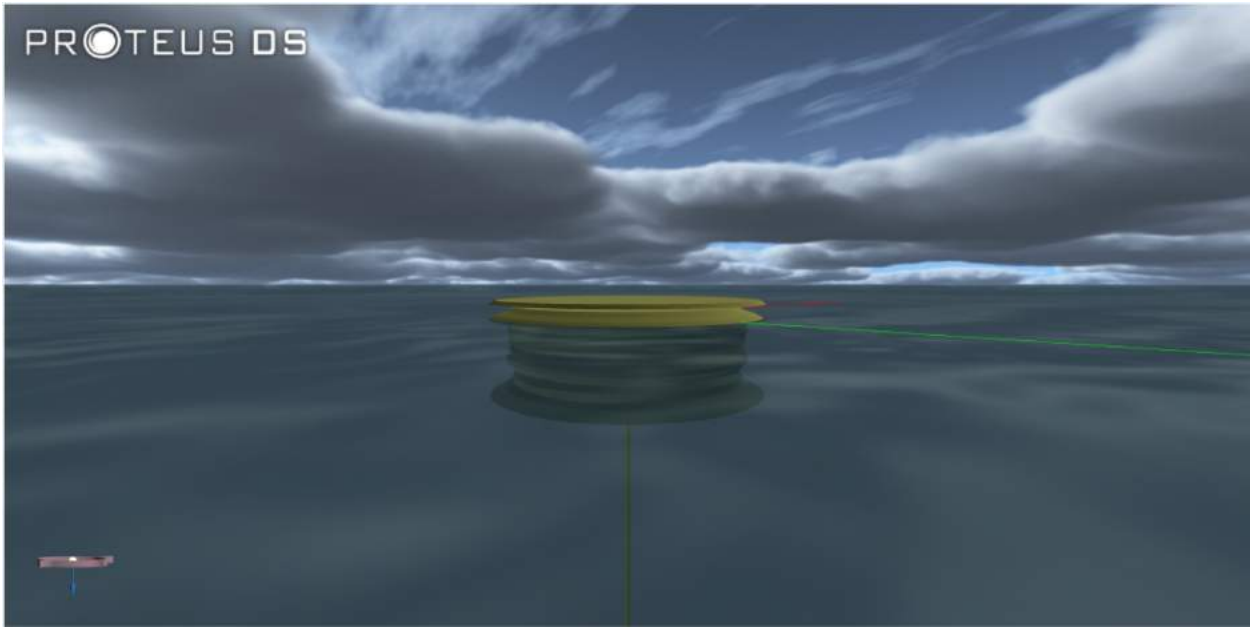

Figure 35 - 100-Generation Shape Evaluated in ProteusDS

The 100-generation hull shape has an estimated average power of 61 W, as evaluated in the ProteusDS miniWEC model with the Lake Washington wave cases. The final hull shape within the miniWEC system improves the average power by 1.94 compared to the baseline cylinder and 3 times the existing miniWEC average power. The proxy predicted the shape would produce 66.8 W*, over-predicting by 10%. Figure 36 shows the power matrix for the 100-generation hull shape.

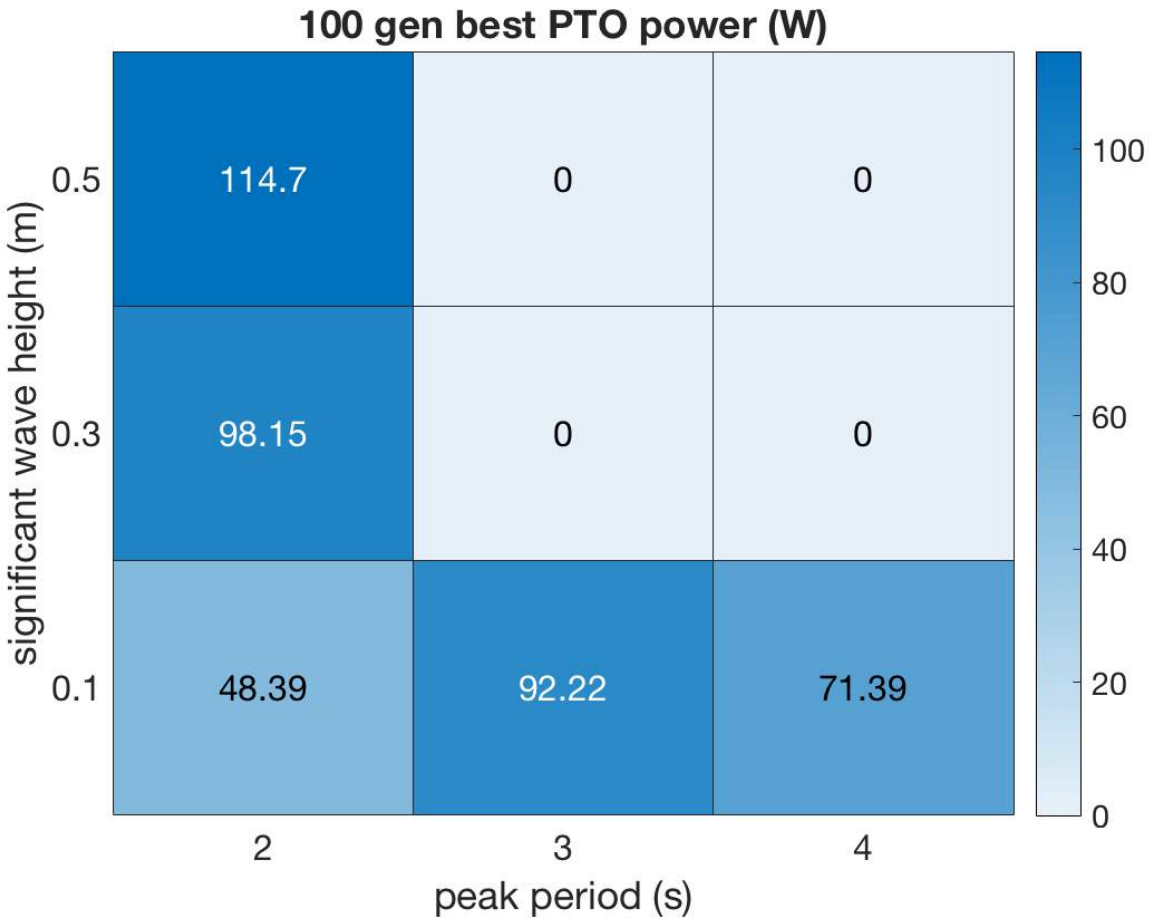

Figure 36 - Final Shape Average Power Bins

The peak power is predicted to be 115 W for the 0.5 m wave height case. The average power in of the 100-generation shape is improved by 2.2 times the average power of the baseline cylinder for the dominant wave case of 0.1m, 2 s, which is the greatest power gain in the power matrix. The annual energy production (AEP) for the final hull shape in the miniWEC system is 550 kWhrs/year. In contrast, the existing miniWEC has an AEP of 175 kWhrs/year. This estimate is based on the results of the ProteusDS model and the wave cases identified by the winter 2012 Lake Washington field data, although the waves are most energetic in winter, so it is likely an overestimate. Finally, the hull vertical position for the 100-generation shape and the cylinder are compared for a ten second interval, with the wave elevation shown for reference (Figure 37).

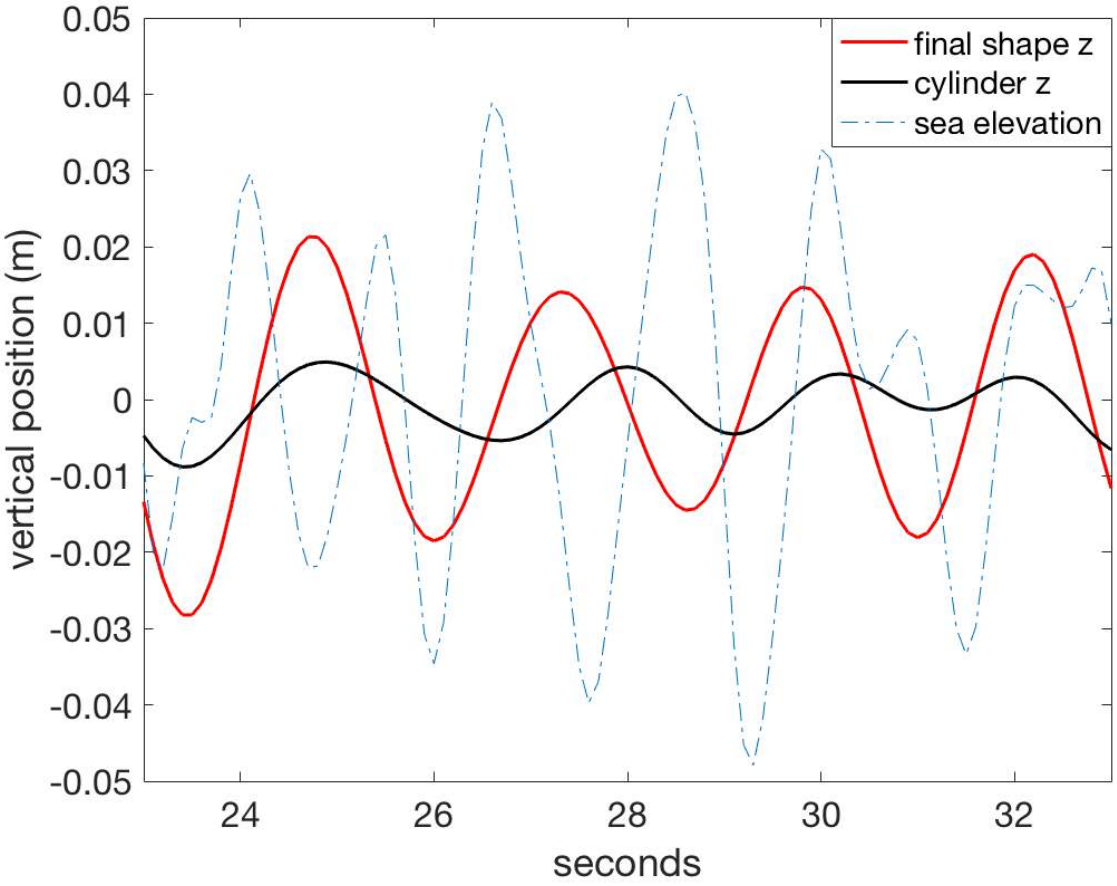

Figure 37 - Heave Amplitude of 100-Generation Shape Compared with Baseline Cylinder (Wave Amplitude Provided for Reference)

The 100-generation hull shape has greater amplitude compared to the baseline cylinder. The 100-generation hull moves with 2.2 times greater heave amplitude compared with the cylinder. The WEC dynamics will vary for each device, but the miniWEC primarily moves in heave motion vertically and produces power proportional to the PTO velocity. The results will now be discussed in further detail.

Chapter 4. DISCUSSION

The genetic algorithm has identified a hull shape that produces significantly more power in Lake Washington compared with the existing miniWEC. The heuristic optimization method is computationally efficient than an approach that includes time domain analysis within the GA. There are many simplifications that contribute to computational efficiency including the axisymmetric shape, the consideration of heave motion exclusively, and the idealized Lake Washington energy spectra. The open-source BEM code NEMOH is used for frequency-domain analysis and an open-source GA toolbox is used to create the GA code, which is provided in the appendix. This method can be implemented for WEC geometry optimization studies in other wave climates.

The empirically derived power proxy is central to identifying high power performing hull shapes with the GA. The power proxy equation matches the time domain power with approximately 10% error for the half of the reference hull shapes and for the 100-generation shape, and effectively promotes the highest power producing shapes and underpredicts the power of the lowest power producing shapes. The GA is able to identify a hull shape that produces twice the average power of a baseline cylinder and three times the average power of the existing miniWEC cylindrical hull. This power increase is promising and may be especially beneficial for WEC developers. The 100-generation hull shape is unique to this case study of the miniWEC in Lake Washington. In particular, the grid search space resulted in jagged profiles rather than having a smoothed spline fit to the geometry, which has been used in other studies [38-39]. It may be beneficial for future studies to use the spline fit so that the geometry identified would be more feasible to manufacture. Additionally, numerical artifacts in the evaluation of the hydrodynamic coefficients in the frequency domain may be generated with an angular profile, and using a spline

fit could reduce the likelihood of such errors. The results are promising for this case study, indicating that the method has significant potential.

4.1 Genetic Algorithm Outcome

The genetic algorithm is run for 100 generations and is able to identify a high power performing hull shape. The 100-generation hull shape is evaluated using the ProteusDS miniWEC model, and is estimated to produces 2 times the power of the baseline cylinder and 3 times the power of the existing miniWEC. The 100-generation hull shape miniWEC system has an average power of 61 W and a peak power of 115 W. The highest power gain occurs in the dominant Lake Washington wave case of 0.1 m height, 2 s period, which shows that the equation is customized for the specific wave climate. The frequency-domain and time-domain analysis of the 50-generation shape follow the same trend as the 100-generation hull shape, which increases confidence in the WEC geometry optimization approach and the power output of the 100-generation hull shape. The best hull shape identified at 50 generations is also evaluated and produces and estimated 52 W which is 1.6 times the power of the cylinder and 2.6 times the power of the existing miniWEC. The PTO velocity is used to estimate the average power of a hull shape, but the hull heave amplitude also describes the system dynamics.

The 100-generation hull shape moves with greater heave amplitude compared with the baseline cylinder. Falnes claims that in order to be a good absorber of wave energy, the device must be a good wave-maker, meaning that WECs should displace water in an oscillating manner with correct phase timing [10]. A heaving point absorber should move with a large amplitude in phase with the waves. It is ideal if the body oscillates with a larger amplitude than the wave [10]. Figure 37 shows that the vertical position of the final hull shape modeled in ProteusDS follows the sea elevation to 71% of the amplitude. This is compared with the baseline cylinder which follows

the sea height vertical position by 32%. The final hull shape does not move in greater amplitude than the sea elevation, but the amplitude is 2.2 times the amplitude of the baseline cylinder. Additionally, the 100-generation hull shape is primarily in the 90° optimal phase angle, indicating that it is a good wave-maker. The optimized hull shape moves with greater amplitude and produces more power than the existing miniWEC system.

The annual energy production of the 100-generation hull shape is approximately 3 times the AEP of the existing miniWEC. The 100-generation hull has an estimated 550 kWhrs/year compared with the existing miniWEC producing an estimated 175 kWhrs/year. The miniWEC is a small device used for research purposes, but the increase in AEP suggests that GA optimization is a valid tool that can be used to improve existing utility scale WECs. A GA can be run for more than 100 generations to get further AEP gains. Increasing the AEP of WECs is crucial for lowering their cost of energy and making them cost competitive with other forms of renewable energy.

4.2 Effectiveness of the Power Proxy

Development of an accurate power proxy is essential to this research. The power proxy equation is a relatively simple, effective way to estimate the power of hull shapes (Equation 3.1). The heave added mass, heave radiation damping, and heave excitation force coefficients are multiplied by idealized energy spectra, the units are standardized to joules, the terms are integrated over the frequency range, empirically weighted, and summed. Though non-physical (and not a response amplitude operator to statistically determine the hull behavior), the power proxy ranks the performance reference hull shapes (Table 2.1). The reference shape analysis demonstrates the trend that high power performing shapes are promoted, average power shapes are accurately estimated, and low power performing shapes are predicted to have low power. However, certain shapes are difficult to fit to the power proxy, such as the reverse disk shape, indicating that there

are indicators of average power that are not being adequately captured by our method. In particular, adding additional terms to the power proxy equation to focus on the dominant 2 s wave period would likely improve the power proxy estimate. The power proxy equation developed in this research study can be applied to other studies, but may need to be adjusted based on the specific WEC search space and wave climate. The power proxy identifies shapes with large excitation force, 90° phase angle, substantial added mass, and minimal damping.

The power proxy is able to identify hull shapes with hydrodynamic coefficients that are optimized in the 1.5 - 4.5 s Lake Washington wave period range. The added mass proxy term for the 100-generation shape is very similar to the added mass proxy term for the baseline cylinder (Figure 31). This indicates that the hull power is not highly correlated with heave added mass for this specific case. The heave radiation damping is minimized (Figure 32), however the negative damping is non-physical. The heave excitation force has the greatest impact on the power proxy equation, and the 100-generation hull shape has an excitation force with a large amplitude and an optimal 90° phase angle in the dominant wave period (Figure 33). Thus, the power proxy is able to identify high power performing hull shapes and the GA is able to strategically search the design space and iterate towards high power performing hull shapes.

4.3 NEMOH Analysis within the Genetic Algorithm

Candidate hull shapes are evaluated in the frequency domain using the open-source BEM code NEMOH. It is important to smooth the NEMOH data by using a filter to ensure that the results are accurate. There are some numerical artifacts resulting in occasional spikes in the hydrodynamic coefficients at a few frequency points. The MATLAB script ‘medfilt1’ is used to smooth the hydrodynamic coefficients so that the data is accurate within the GA. This results in greater precision of the power proxy comparison to time domain power, and more realistic data

points throughout the entire frequency range. The accuracy of the hydrodynamic coefficients is important because the data is being input into the time domain models.

Many mid-fidelity time domain models are capable of incorporating hydrodynamic data from separate BEM solvers. The 50-generation shape and 100-generation shape are evaluated in the ProteusDS miniWEC model using the NEMOH hydrodynamic coefficients. However, it would be interesting to validate the average power through other methods, such as a different BEM code, a higher fidelity CFD model, scaled tank testing, or full-scale field testing.

4.3.1 *Geometric Smoothing of 100-Generation Shape*

The 100-generation hull shape is geometrically smoothed to identify if the hull shape can be more easily manufactured and still produce a similar power output. The MATLAB function medfilt1 is used to smooth the points that define the 100-generation shape profile. The filter outputs the same number of points as the input data, the 26 radial points that define the search space. Figure 38 shows the filtered points compared with the final hull shape from 100 generations.

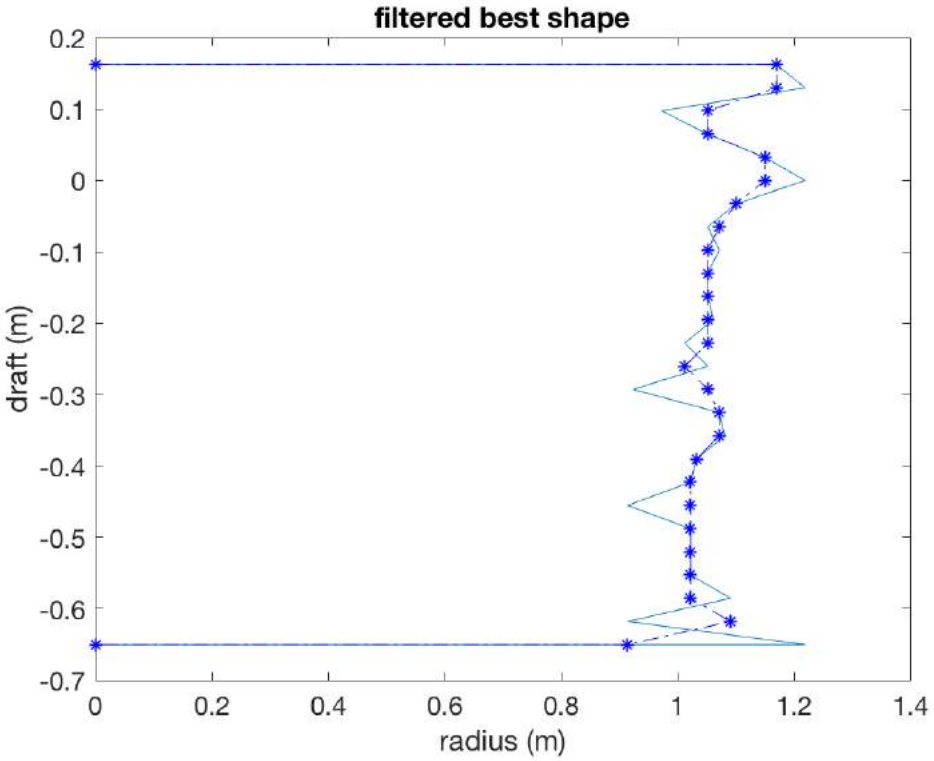

Figure 38 - Filtered Final Shape

The smoothed hull shape is evaluated using NEMOH and the ProteusDS miniWEC model. The frequency-domain analysis of the filtered shape more closely resembles the highest power producing reference shapes rather than the 100-generation shape. The smoothed shape is estimated to produce 34 W of average power, which is significantly less than the 61 W produced by the 100-generation shape. This may be due to numerical artifacts in NEMOH. However, it may also be a result of too much smoothing. For instance, the large radial spike at the base is not captured, but is quickly converged on within the GA. The geometrically smoothed hull shape power output indicates that the fine geometric detail is important for power production. Additionally, it indicates that geometric smoothing within the GA would be more effective than geometric smoothing of a result that is identified on a grid. Figure 39 shows the power matrix for the smoothed shape.

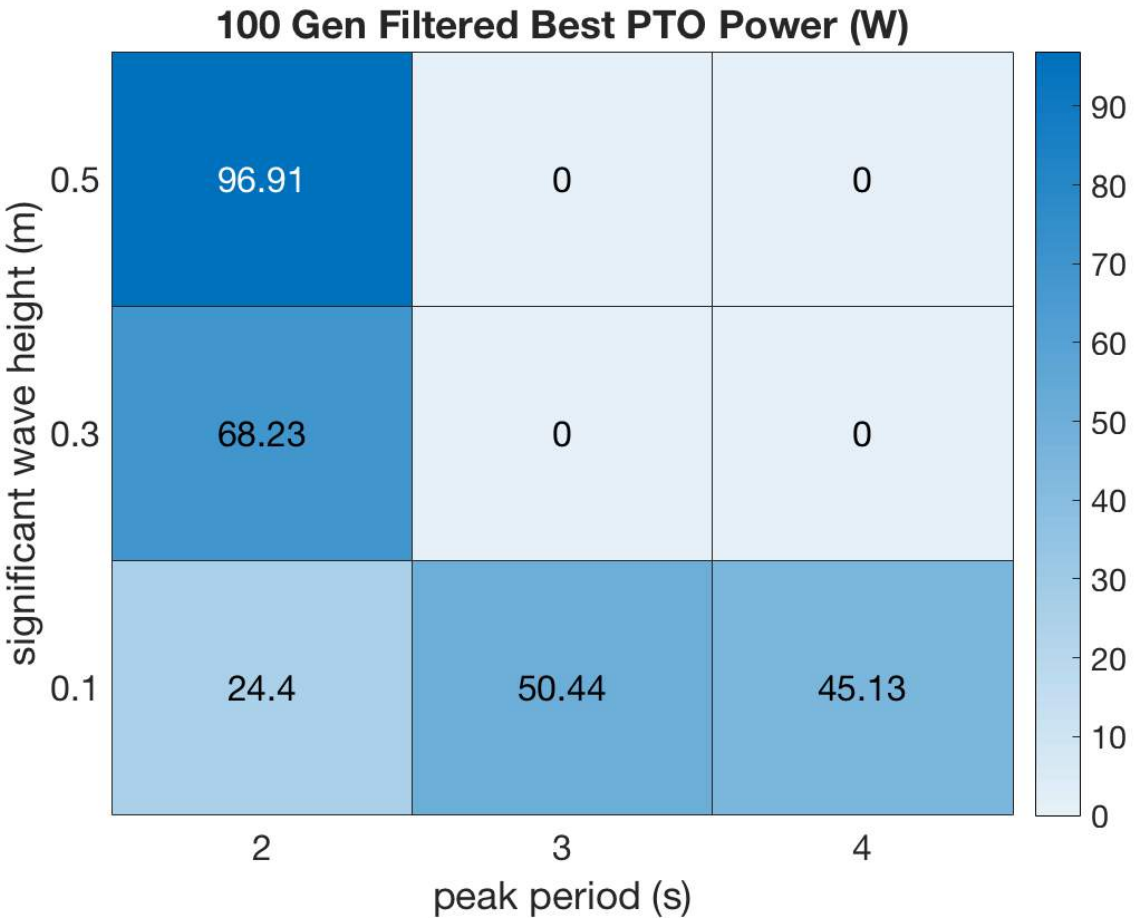

Figure 39 - Average Power per Wave Case for Filtered Best Shape

4.3.2 *Computational Time*

This method provides a computationally efficient way to identify high power performing WEC hull shapes, with the flexibility to modify the code for different applications. An exhaustive search would not be feasible, iterative methods of design and evaluate would likely not find an optimal hull geometry, and including time domain analysis within the GA would be too time intensive with our computational capabilities. Although this research implements many geometric simplifications and frequency-domain analysis, the time to run the GA is still significant. The GA runs on a windows laptop with 4 CPUs in a MATLAB environment. The GA takes almost 6 weeks

to progress over 100 generations evaluating each candidate shape sequentially. Implementing the MATLAB parallel computing toolbox significantly speeds up computational time [57]. Four hull shapes are evaluated simultaneously using the 4 cores of the laptop. Using this method, 100 generations can be evaluated in approximately 10 days. With greater computational capabilities it would be possible to evaluate all 30 candidate hull shapes in NEMOH in parallel. This is possible with access to a data center or by modifying the code to run on the cloud. Cloud computing was considered, however the NEMOH executable files would need to be modified and this is outside the scope of this research. MATLAB's parallel computing toolbox provides significant computational efficiency, and reducing computational time further is an area of future work.

4.4 Investigation of Evolved Geometries

The shapes that the GA identifies have the maximum radius at the waterline and hull base, with rigid features between. There is a significant increase in power proxy from 70 to 71 generations, followed by incremental power proxy gains to 100 generations. Figure 40 shows the profile for the 70-generation and 71-generation shapes.

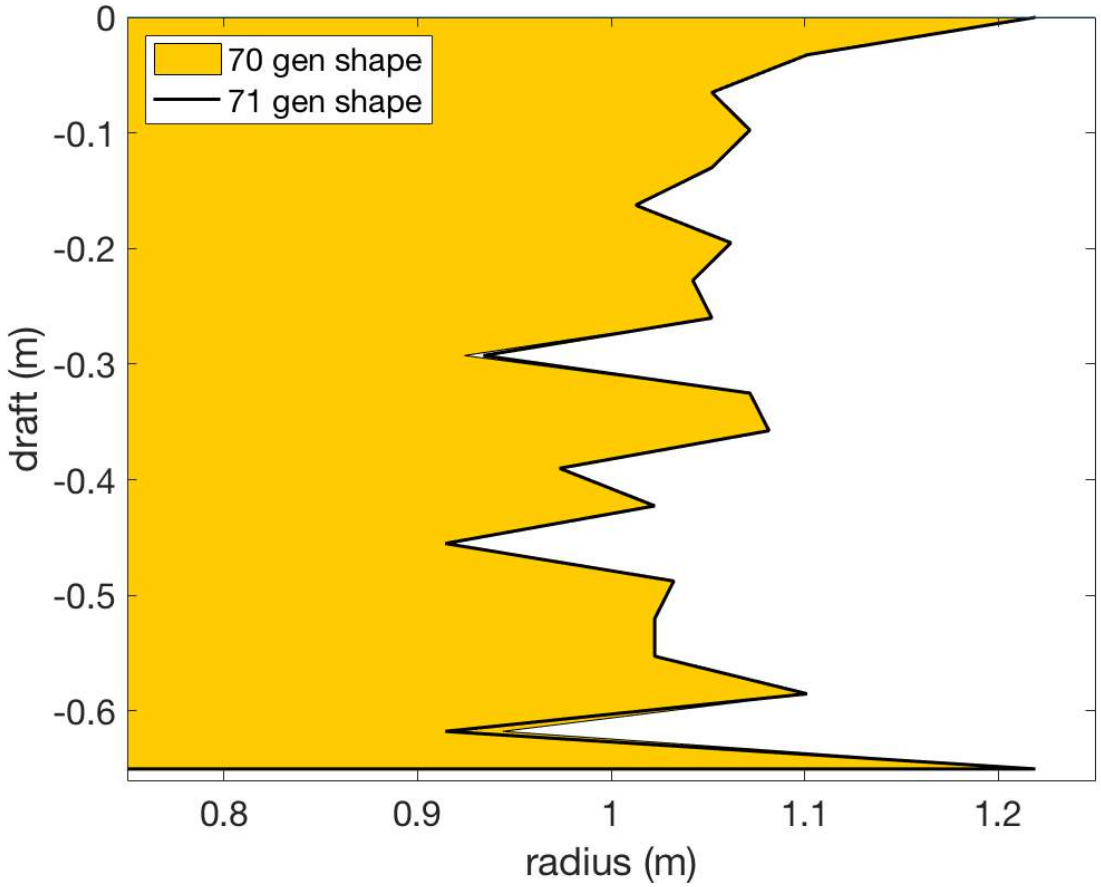

Figure 40 - Shape Profile Change 70 to 71 Generations (2% Proxy Increase followed by Proxy Convergence)

There is very little difference between the 70-generation and 71-generation shapes. The most significant change is the reduction in radius from 0.9439 m to 0.9144 m at 0.6177 m draft. There is also a slight radial increase at 0.2926 m draft, but this position later moves back. Figure 41 shows the profiles at 70 and 71 generations in addition to the 100-generation shape profile.

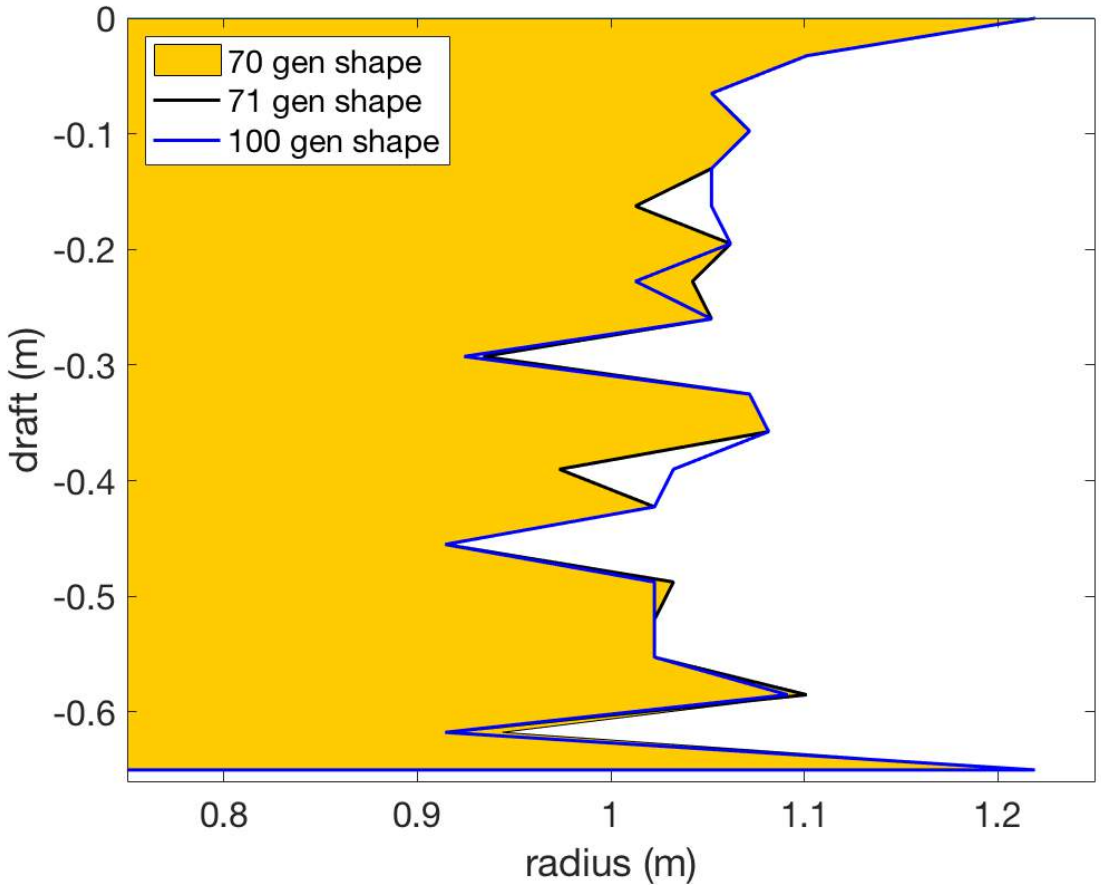

Figure 41 - Profile at 70 Generations, 71 Generations, and 100 Generations (Proxy Increases by 2% between 70 and 71 Generations, and then less than 2% increase towards 100 Generations)

The final hull shape at 100 generations has some significant changes to the profile as compared to the 70 and 71 generation shapes. In particular, the central fin has a smoother profile with a larger angle between the points, and there is a similar change above this feature. It is surprising that the small feature change between 70 to 71 generations has a more significant impact to the power proxy than the larger profile changes at 100 generations. This may be due to a numerical error resulting from the mesh. Future work can modify the mesh within the NEMOH code. Additionally, further shape sensitivity studies may indicate that a courser grid is needed or that a spline fit would be beneficial to avoid the sharp corners.

The results of the sensitivity study show that more sensitivity analysis is required to have full confidence in the search space. There are additional reasons to implement a spline fit, especially considering manufacturability and cost. The sensitivity study does show that the radial position of the hull at the waterline has a large impact on the excitation force. The excitation force for the shapes with greatest radius at the waterline is similar to the excitation force for the maximum radius cylinder. In contrast, the two spikey shapes with minimum radius at the waterline have very low excitation force amplitude. This seems to support the GA converging towards a shape with the maximum radius at the waterline, especially since the excitation force has the largest impact on the power proxy.

The genetic algorithm shapes are unique to this case study, but the method can be applied to other research studies. Heuristic optimization methods applied to WEC geometry can contribute to significant advances in this area by indicating optimal hull shapes for wave energy conversion. The size and scale of WECs need to be tuned to the resonant frequency of local wave climates, however certain archetypes of hull shapes for types of WECs could emerge to indicate power enhancement based on geometric shape. Heuristic optimization methods may identify hull geometries which are ideal in real ocean conditions.

4.5 Practical Considerations

The manufacturability of the hull shape is an important practical consideration. Ideally, the best hull shape could be added to the existing miniWEC hull as a foam layer that surrounds the 0.91 m radius cylinder. The 100-generation hull shape has many unique features and would likely be expensive to manufacture. Unfortunately, the geometrically smoothed shape did not produce enough power to make it worthwhile compared with the reference shapes. Thus, it would be better to incorporate geometric smoothing through a spline fit within the GA so that the hull shape

identified would be feasible to manufacture. However, the power gains demonstrated over 100-generations shows that this method has promise and further modifications can make it more applicable to the hull design of commercial WECs.

The study demonstrates that the power can be increased by a factor of three in this case, with around 550 kWhrs/year compared with 175 kWhrs/year. Average power gains of 3 times and greater would be significant for commercial WEC developers. Future studies could be evaluated for more generations to produce greater power gains, and additional constraints on the hull shape could result in more manufacturable shapes. An increased capital cost of manufacturing a hull shape identified by a GA, could be justified by the gains in AEP that could be generated through an evolved geometry.

Chapter 5. CONCLUSION

Heuristic geometry optimization methods can be used to improve the economic viability of WECs. The broader goals of developing a computationally cost effective, frequency-domain-based hydrodynamic WEC geometry optimization method have been achieved and demonstrated through a case evaluation with promising results. The code has been made publicly available on github and is also shown in the appendix. This method can be used for other WEC geometry optimization studies. The geometry search space and local wave climate can be adjusted based on specific project goals. The results of this research study support the use of wave energy converters to sustainably contribute to renewable energy solutions, in combination with reductions in energy usage to mitigate the effects of climate change.

There are many opportunities for future work in this research area. This research provides a simple case evaluation, however the geometry search space could be expanded to include the base

so that shapes may have rounded rather than flat bases. Other components, such as surge and pitch motion, could also be included in addition to heave. Further complexity could be added to include non-axisymmetric and 3D shapes, in addition to adding a spline fit to help the GA converge to manufacturable geometries while optimizing for power. A hull shape with three times the power output has been achieved through 100 generations of running a GA with frequency-domain analysis using the open-source code NEMOH. This research study provides a computationally efficient methodology for other studies to use and expand upon.

The empirical power proxy identifies high power producing hull shapes based on their heave hydrodynamic coefficients. The added mass, radiation damping, and excitation force amplitude and phase angle are used within the objective function to evaluate and rank fitness of hull shapes within the GA. It is important to validate these results using CFD, scaled tank testing, or field testing in Lake Washington. Additionally, the empirical power proxy could be further refined by evaluating more data and including additional metrics for average power.

This research study contributes to a methodology to optimize wave energy hull shapes for annual average power. Although these methods focus on a specific geometry, results can be compared to indicate paths forward for other WEC hull geometry optimization, advancing wave energy research and development.

BIBLIOGRAPHY

[1] A. Finlay, L. Watts and A. Peebles, “ebban an’ flowan.” Edinburgh: *morning star*, ISBN 978-1904477150, 2015, pp. 8-15.

[2] Gunn, K. and Stock-Williams, C. (2012). Quantifying the global wave power resource. *Renewable Energy*, 44, pp.296-304.

[3] “Living Ocean Science Mission Directorate", *Science.nasa.gov*, 2018. [Online]. Available: https://science.nasa.gov/earth-science/oceanography/living-ocean.

[4] Paris United Nations (2015). *Paris Agreement*. United Nations Framework Convention on Climate Change. [online] Available at: https://unfccc.int/process-and-meetings/the-paris-agreement/the-paris-agreement.

[5] J. Weber, D. Laird, C. Ronan, B. Kennedy, J. Roberts, D. Bull, A. Babarit, K. Nielsen and C. Bittencourt Ferreira, “Cost, Time, and Risk Assessment of Different Wave Energy Converter Technology Development Trajectories”, *European Wave and Tidal Energy Conference*, 2017.

[6] Strategic Initiative for Ocean Energy (2012). *Ocean Energy: State of the Art*.

[7] L. Sjokvist, M. Goteman, M. Rahm, R. Waters, O. Svensson, E. Stromstedt, and M. Leijon. “Calculating buoy response for a wave energy converter – A comparison of two computational methods and experimental results.” Theoretical and Applied Mechanics Letters Vol. 7 (2017): pp. 164-168. URL http://creativecommons.org/licenses/by-nc-nd/4.0/.

[8] J. Cruz. Ocean Wave Energy, Current Status and Future Perspectives. *Springer, Green Energy and Technology*, Bristol, 2008.

[9] J. Falnes. Ocean Waves and Oscillating Systems, Linear Interactions Including Wave Energy Extraction. *Cambridge University Press*, Cambridge, 2004.

[10] J. Falnes, “Principles for Capture of Energy from Ocean Waves. Phase Control and Optimum Oscillation”, *Department of Physics, NTNU, Trondheim, Norway*.

[11] Newman, J. (1977). *Marine Hydrodynamics*. MIT Press.

[12] LHEEA Centrale Nantes, "General Notations and Conventions", Nantes, 2014.

[13] J. Luoma, "Capturing the Ocean’s Energy", *Yale E360*, 2018. [Online]. Available: https://e360.yale.edu/features/capturing_the_oceans_energy.

[14] Aquaret.com. (2018). *Welcome to Aqua-RET*. [online] Available at: http://aquaret.com/

[15] Magagna, D., Uihlein, A., Silva, M. and Raventos, A. (2015). Wave and tidal energy in Europe: assessing present technologies. In: *EWTEC*. Nantes: European Wave and Tidal Energy Conference, pp.1-6.

[16] CorPower Ocean. (2018). *The CorPower Wave Energy Converter - CorPower Ocean*. [online] Available at: http://www.corpowerocean.com/corpower-technology/corpower-wave-energy-converter/.

[17] Oscillapower.com. (2018). *Oscilla Power – Generating Power with Ocean Waves*. [online] Available at: https://oscillapower.com/

[18] Boltseapower.com. (2018). *www.boltseapower.com*. [online] Available at: http://www.boltseapower.com/

[19] Oceanpowertechnologies.com. (2018). *Powerbuoy Technology*. [online] Available at: https://www.oceanpowertechnologies.com/powerbuoy [Accessed 1 Jun. 2018].

[20] S. Salter. "Wave Energy: Nostalgic Ramblings, future hopes and heretical suggestions." *Journal of Ocean Engineering and Marine Energy* Vol. 2 (2016): pp. 399-407. DOI 10.1007/s40722-016-0057-3.

[21] A. Price, C. Dent and A. Wallace, "Frequency domain techniques for numerical and experimental modeling of wave energy converters", Proceedings of the 8th European Wave and Tidal Energy Conference, Uppsala, Sweden, pp. 849-858, 2009.

[22] WAMIT Inc, The State of the Art in Wave Interaction Analysis, URL http://www.wamit.com/publications.htm, Chestnut Hill, MA, 2016.

[23] B. BEMs, "Battle of the BEMs", *Wavepowerconundrums.com*, 2014. [Online]. Available: http://www.wavepowerconundrums.com/2014/02/battle-of-the-bems.html.

[24] Ansys.com. (2018). *ANSYS Aqwa: Hydrodynamics Simulation & Diffraction Analysis*. [online] Available at: https://www.ansys.com/products/structures/ansys-aqwa

[25] A. Babarit and G. Delhommeau. "Theoretical and Numerical Aspects of the open source BEM solver NEMOH." *Proceedings of the 11th European Wave and Tidal Energy Conference*. Nantes, France. 2015. URL http://hal.archives-ouvertes.fr/LHEEA/hal-01198800.

[26] Dynamic Systems Analysis Ltd. "ProteusDS Manual." Victoria, BC, Canada. 2017.

[27] "Orcina: OrcaFlex", *Orcina.com*, 2018. [Online]. Available: https://www.orcina.com/SoftwareProducts/OrcaFlex/.

[28] "WEC-Sim (Wave Energy Converter SIMulator) — WEC-Sim documentation", *Wec-sim.github.io*, 2018. [Online]. Available: https://wec-sim.github.io/WEC-Sim/.

[29] Ocean Energy Systems (2016). *Task 10: Wave Energy Converters Modelling Verification and Validation*. [online] Lisbon. Available at: https://www.ocean-energy-systems.org/oes-projects/task-10-wave-energy-converters-modelling-verification-and-validation/#tab-results.

[30] "Standards: EMEC European Wave Energy Centre", *Emec.org.uk*, 2018. [Online]. Available http://www.emec.org.uk/standards/.

[31] "ANSYS Fluent Software: CFD Simulation", *Ansys.com*, 2018. [Online]. Available: https://www.ansys.com/products/fluids/ansys-fluent.

[32] "STAR-CCM+ | MDX", *Mdx.plm.automation.siemens.com*, 2018. [Online]. Available: https://mdx.plm.automation.siemens.com/star-ccm-plus.

[33] "OpenFOAM&#174 - Official home of The Open Source Computational Fluid Dynamics (CFD) Toolbox", *Openfoam.com*, 2018. [Online]. Available: https://www.openfoam.com/.

[34] P. Kelly Senecal, "Numerical Optimization using the Gen4 Micro-Genetic Algorithm Code", *Engine Research Center, University of Wisconsin Madison*, 2000.

[35] A. Babarit, A. Clement, J. Ruer, and C. Tartivel. "SEAREV: A Fully Integrated Wave Energy Converter." *Proceedings of the OWEMES*. Rome, April, 2006. URL https://pdfs.semanticscholar.org/6384/764f4984381b8cde9563dfe238477f647276.pdf.

[36] T. Mundon. "Optimising the Output of an Articulated WEC Through the Use of a Biologically-Inspired and Artificially Evolved Neural Network," PhD Thesis. *University of Edinburgh*, Scotland. 2006.

[37] K. Gunn, J. Taylor, and C. Lingwood. "Evolutionary Algorithms for the Development and Optimisation of Wave Energy Converter Control Systems." *Proceedings of the 8th European Wave and Tidal Energy Conference*. pp. 697-706. Uppsala, Sweden, September 7-10, 2009. URL http://www.homepages.ed.ac.uk/shs/Wave%20Energy/EWTEC%202009/EWTEC%202009%20(D)/papers/274.pdf.

[38] A. McCabe. "Constrained Optimization of the Shape of a Wave Energy Collector by Genetic Algorithm." *Renewable Energy* Vol. 51 (2013): pp. 274-284. URL http://dx.doi.org/10.1016/j.renene.2012.09.054.

[39] A. Garcia Teruel, D. Forehand, H. Jeffrey, and A. de Andres, "Cost and Performance Optimization of Wave Energy Converters." *Institute for Energy Systems Research Conference*. pp. 1-18. University of Edinburgh, Scotland, 2016. URL https://www.youtube.com/watch?v=mAA812TW7Kw.

[40] R. Gomes, J. Henriques, L. Gato, and A. Falcao. "Hydrodynamic Optimization of an Axisymmetric Floating Oscillating Water Column for Wave Energy Conversion." *Renewable Energy* Vol. 44 (2012): pp. 328-339. DOI 10.1016/j.renene.2012.01.105

[41] C. Sharp, B. DuPont, B. Bosma, P. Lomonaco, and B. Batten. "Array Optimization of Fixed Oscillating Water Columns for Active Device Control." *Proceedings of the 12th European Wave and Tidal Energy Conference*. Paper #1016. pp. 1-10. Cork, Ireland, August 27 – September 1, 2017. URL https://www.researchgate.net/publication/319406762_Array_Optimization_of_Fixed_Oscillating_Water_Columns_for_Active_Device_Control.

[42] J. Ortiz, H. Bailey, B. Buckham, and C. Crawford. "Surrogate Based Design of a Mooring System for a Self-reacting Point Absorber." *Proceedings of the Twenty-Fifth International Ocean and Polar Engineering Conference*. pp. 936-943. Kona, Hawaii, USA. June 21-26, 2015.

[43] H. Bailey, B. Robertson and B. Buckham. "Optimizing WECs for Canadian Waters." *Proceedings of the International Conference on Ocean Energy*. Halifax, Nova Scotia, Canada, Nov 4-6, 2014. URL http://www.icoe2014canada.org/wp-content/uploads/2014/11/BaileyHelenARTICLE_14-4.pdf.

[44] D. Sale, A. Aliseda, M. Motley, and Y. Li, "Structural Optimization of Composite Blades for Wind and Hydrokinetic Turbines", *Proceedings of the NHA Marine Energy Technology Symposium.*, pp. 1-10, Washington, DC.

[45] A. Dallman and V. Neary, "Characterization of U.S. Wave Energy Converter (WEC) Test Sites: A Catalogue of Met-Ocean Data." SAND2015-7963. *Sandia National Labs*,

Albuquerque, New Mexico. 2015. URL https://openei.org/w/images/9/90/SNL_US_WEC_TestSiteCatalogue_2ndEdition_Part1.pd

[46] K. Hasselmann, T. Barnett, E. Bouws, H. Carlson, D. Cartwright, K. Enke, J. Ewig, H. Gienapp, D. Hasselmann, P. Kruseman, A. Meerburg, P. Muller, D. Olbers, K. Richter, W. Sell and H. Walden, "Measurements of Wind-Wave Growth and Decay during the Joint North Sea Wave Project (JONSWAP)", Deutsches Hydrographisches Institut, Hamburg, 1973.

[47] WAFO-group. "WAFO – A Matlab Toolbox for Analysis of Random Waves and Loads – A Tutorial." *Math. Stat., Center for Math. Sci., Lund Univ*., Lund, Sweden. URL http://www.maths.lth.se/matstat/wafo

[48] "Datawell BV - Home of the Waverider", *Datawell.nl*, 2018. [Online]. Available: http://www.datawell.nl/.

[49] J. Thomson, "Lake WA waveriders." faculty.washington.edu. 2012.

[50] A. Brown and J. Thomson, "Phase-resolved heave plate dynamics for wave energy converters", *Proceedings of the NHA Marine Energy Technology Symposium*. pp. 1-5. Washington, DC, 2016. URL https://depts.washington.edu/nnmrec/docs/METS2016_Brown.pdf

[51] "1-D median filtering – MATLAB medfilt1", *Mathworks.com*, 2018. [Online]. Available: https://www.mathworks.com/help/signal/ref/medfilt1.html.

[52] J. Giagkiozis, R. Purshouse and P. Fleming. "An Overview of Population-Based Algorithms for Multi-Objective Optimization." *International Journal of Systems Science* Vol. 00 No. 00, (2013): pp. 1-42. URL http://dx.doi.org/10.1080/00207721.2013.823526.

[53] Rusch, C. (2018). *miniWEC Proteus Modeling*. Seattle, pp.1-14.

[54] Rosenberg, B., Mundon, T., Cavagnaro, R., Rusch, C., Maurer, B., Thomson, J. and Polagye, B. (2018). Development and Field Testing of PTO Control Strategies for Two-Body Flexibly-Connected WECs. Washington D.C.: Marine Energy Technology Symposium, pp.1-4.

[55] A. Chipperfield, P. Fleming, H. Pohlheim and C. Fonseca, "Genetic Algorithm TOOLBOX Document: for use with MATLAB."

[56] Datta, S., Genetic Algorithm in MATLAB for Process Optimization Multi-objective Approch for Optimization, ChE Thoughts 2 (2), 25-29, 2011.

[57] "Parallel Computing Toolbox", *Mathworks.com*, 2018. [Online]. Available: https://mathworks.com/products/parallel-computing.html.

[58] "Rhino 6 for Windows", Rhino3d.com, 2018. [Online]. Available: https://www.rhino3d.com/.

APPENDIX. GENETIC ALGORITHM CODE

GitHub URL: https://github.com/Kayliemct/Genetic-Algorithm-for-WEC-Design.git

GA_shapes_v2.m | objfunShapes2.m | axiMeshGA2.m | NemohEval.m | NemohGA2.m

```
% GA_shapes_v2.m     % Genetic algorithm for optimal miniWEC float shape KM

clear all; close all; clc

%% GA parameters
Nind = 30;                          % micro GA w/ 30 individuals
NVAR = 26;                          % number of variables
PRECI = 5;                          % discrete increments - 32 with 0.0098m spacing
MAXGEN = 25;%50;                        % increase MAXGEN after preliminary runs
GGAP = 0.9;                         % generational gap

% field descriptor
FieldD = [rep([PRECI],[1,NVAR]);rep([0.9144;1.2192],[1,NVAR]);...
    rep([1;0;1;1],[1,NVAR])];                                   % Gray coded

% initial population
Chrom = crtbp(Nind,NVAR*PRECI);

% seed initial population with ellipse, rev disk, and rev conical
Chrom(1,:) = [0,0,0,0,0,0,0,1,1,0,0,1,1,0,0,0,1,0,1,0,1,1,0,0,0,1,1,1,1,0,1,1,1,0,0,1
Chrom(2,:) = [1,0,0,0,0,1,0,0,1,1,1,0,1,1,1,1,1,1,0,0,1,1,1,1,0,1,1,0,1,1,0,1,0,0,0,0
Chrom(3,:) = [1,0,0,0,0,1,0,0,0,1,1,0,0,1,1,1,0,1,1,0,1,0,1,1,1,1,0,1,0,1,1,1,1,0,0,1

% Reset counters
   Best = NaN*ones(MAXGEN,1);   % best in current population
   global R_data P_data Z_data
   gen = 0;                     % generational counter
   R_data = zeros(1,28);        % stores radius data
   Z_data = zeros(1,28);
```

GA_shapes_v2.m | objfunShapes2.m | axiMeshGA2.m | NemohEval.m | NemohGA2.m

```
30 -     P_data = 0;                  % stores power proxy data
31 -     go = char('go');             % read in 'stop' or 'go' within loop
32 -     tic;
33
34 -   parpool parallel computing
35 -     parpool('local',4);                                        %parallel computin
36 -     options = optimoptions('ga','UseParallel', true, 'UseVectorized', false);    %
37
38     % Evaluate initial population, call NEMOH in objfunShapes.m
39 -     ObjV = objfunShapes2(bs2rv(Chrom,FieldD));
40
41     % Generational Loop
42 -   while (gen < MAXGEN & char(go) == 'go')
43
44         % read text file -> 'stop' or 'go' to terminate in real time
45 -       [go] = textread('StopGA.dat',...
46             '%s');
47
48         % Assign fitness values to population (minimizing based on '50000-Proxy.*10')
49 -       FitnV = ranking(ObjV);
50
51         % Select individuals for breeding (stochastic universal sampling)
52 -       SelCh = select('sus', Chrom, FitnV, GGAP);
53
54         % Recombine individuals (single point crossover)
55 -       SelCh = recombin('xovsp',SelCh,0.7);
56
57         % Mutate
58 -       SelCh = mut(SelCh);
```

GA_shapes_v2.m | objfunShapes2.m | axiMeshGA2.m | NemohEval.m | NemohGA2.m

```
58 -        SelCh = mut(SelCh);
59
60          % Evaluate Offspring, call NEMOH in objfunShapes.m
61 -        ObjVSel = objfunShapes2(bs2rv(SelCh,FieldD));
62
63          % Reinsert Offspring into population
64 -        [Chrom, ObjV] = reins(Chrom, SelCh, 1, 1, ObjV, ObjVSel);
65
66          % Plot best shape fitness function & profile
67 -        clear prof
68 -        [Best(gen+1),I] = min(ObjV);
69 -        figure(1)
70 -        subplot(1,2,1)
71 -        plot(Best,'bo');
72 -        hold on
73 -        plot(49423,'rx')        %best Proxy of preliminary shapes - teardrop %check**
74 -        xlabel('generation'); ylabel('fitfun(x)');
75 -        text(0.5,0.95,['Best = ', num2str(round(Best(gen+1)))],'Units','normalized');
76 -        hold off
77 -        subplot(1,2,2)
78 -        prof = bs2rv(Chrom(I,:),FieldD);   %plot best shape of each generation
79 -        area(prof);
80
81          % Increment counter
82 -        gen = gen+1;
83
84 -    end
85
86 -    toc
```

GA_shapes_v2.m | objfunShapes2.m | axiMeshGA2.m | NemohEval.m | NemohGA2.m

```
% objfunShapes.m - objective function to use with GA_shapes_v1.m KM

% check if shape has already been evaluated & locate proxy
% run NEMOH using 'axiMeshGA.m' & 'NemohGA.m'
% low pass filter on data
% power proxy = a(MaSj/T^2)+b(DSjT)+c(a(Ex)Sj*sin(phase))
% fitness function = abs(50000-proxy.*10)'

function ObjValS = objfunShapes2(Chrom,FieldD);

global R_data P_data Z_data

% Compute population parameters
   [Nind,Nvar] = size(Chrom);
%    save('Chrom.mat','Chrom');    %overwrites previous population chrom.mat

% pre-NEMOH evaluation
for i = 1:Nind

    datadir = ['C:\Users\labuser\Documents\Kaylie\GA\100GenParallel\',sprintf('%d',i)];
    cd (datadir);        %change directory for each individual

    % radius data points
    r = [0, Chrom(i,1:26), 0];

% vertical spacing for float & number of points for NEMOH
    z = [0.8128, linspace(0.8128,0,26), 0];
    n = 28;

```

Editor - C:\Users\labuser\Documents\Kaylie\GA\100GenParallel\objfunShapes2.m

GA_shapes_v2.m | objfunShapes2.m | axiMeshGA2.m | NemohEval.m | NemohGA2.m

```
30      % find draft for equivalent submerged volume through numerical integration
31 -        Vol_Z = 0;              % for summing volume of the slices
32 -        dZ = z(1,end-4)-z(1,end-3);     % height of slices
33 -        rad = fliplr(r);      % start num. int. from base of shape
34
35 -        for k=2:length(z)-2
36 -        Radius_k = rad(1,k);
37 -        Area_k = pi().*Radius_k.^2;
38 -        Volume_k = Area_k.*dZ;
39 -        Vol_Z = Vol_Z + Volume_k;
40 -        if Vol_Z >2.145                % select the draft closest to volume 2.145 m^3
41 -            error1 = Vol_Z-2.145;
42 -            error2 = Vol_Z-Volume_k-2.145;
43 -            if abs(error1) < abs(error2)
44 -                d = k.*dZ;
45 -                break
46 -            else
47 -                d = (k-1).*dZ;
48 -                break
49 -            end
50 -        end
51 -        end
52
53      % subtract draft from vertical spacing to get z & find vertical centroid
54 -        z = z-d;
55 -        polyin=polyshape({r},{z});
56 -        [x_c,zCG]=centroid(polyin);
57
```

GA_shapes_v2.m | objfunShapes2.m | axiMeshGA2.m | NemohEval.m | NemohGA2.m

```
% evaluate using NEMOH pre-processing - axiMeshGA.m
    [m,M_nemoh,KH,XB,YB,ZB] = axiMeshGA2(r,z,n,zCG,i);

% saving z data for each shape
    u0 = size(R_data,1);
    u = u0+i+1;     %space between generations
    Z_data(u,:) = z;
end

% back to main directory
    cd ('C:\Users\labuser\Documents\Kaylie\GA\100GenParallel\');

% parallel loop running NEMOH
parfor p = 1:Nind

    Proxy(p) = NemohEval(p);

end

% Fitness function to be minimized
    ObjValS = abs(50000-Proxy.*10)'; %max Proxy = 5,000 with this fitness function

% save r and Proxy for future repeated shapes to solve faster
    u0 = size(R_data,1);
    for j=1:Nind
        u = u0+j+1;                 % space between offspring generations
        R_data(u,:) = [0, Chrom(j,:), 0];
        P_data(u) = Proxy(j);
    end
end
```

GA_shapes_v2.m | objfunShapes2.m | axiMeshGA2.m | NemohEval.m | NemohGA2.m

```
%
% --> function [Mass,Inertia,KH,XB,YB,ZB]=axiMesh(r,z,n)
%
% Purpose : Mesh generation of an axisymmetric body for use with Nemoh
%
% Inputs : description of radial profile of the body
%   - n         : number of points for discretisation
%   - r         : array of radial coordinates
%   - z         : array of vertical coordinates
%
% Outputs : hydrostatics
%   - Mass      : mass of buoy
%   - Inertia   : inertia matrix (estimated assuming mass is distributed on
%   wetted surface)
%   - KH        : hydrostatic stiffness matrix
%   - XB,YB,ZB  : coordinates of buoyancy center
%
% Warning : z(i) must be greater than z(i+1)
%
% Copyright Ecole Centrale de Nantes 2014
% Licensed under the Apache License, Version 2.0
% Written by A. Babarit, LHEEA Lab.
%
function [Mass,Inertia,KH,XB,YB,ZB]=axiMeshGA2(r,z,n,zCG,p)
rho=1000;               %fresh water or seawater
g=9.81;
ntheta=50;              %50 sections
name=sprintf('%d',p);   %Individuals in a population are saved in separate folders, repeated each gen
nPanel=500;             %500 target panels
```

GA_shapes_v2.m | objfunShapes2.m | axiMeshGA2.m | NemohEval.m | NemohGA2.m

```
% function NemohEval.m - NEMOH with parallel computing %KM

function Proxy = NemohEval(p)

    datadir = ['C:\Users\labuser\Documents\Kaylie\GA\100GenParallel\',sprintf('%d',p)];
    cd (datadir);        %change directory for each individual

% evaluate using NEMOH - NemohGA.m
    w = linspace((2*pi()./8),(2*pi()./0.5));
    clear A B Fe
    [A,B,Fe] = NemohGA2(w,p);

% get desired added mass and damping data
    for jj=1:6
        a(jj,:) = A(jj,jj,:);
        b(jj,:) = B(jj,jj,:);
    end

% Filter NEMOH data - heave only
    af = medfilt1(a(3,:));
    bf = medfilt1(b(3,:));
    FefA = medfilt1(abs(Fe(:,3)));
    Fefph = medfilt1(angle(Fe(:,3)))+pi();

% Power proxy = a(MaxSj)+b(DxSj)+c(ExxSj)
    Hmo = 0.18;
    Tp = 1.5;
    gamma = 3.3;        %3.3 for Jonswap
    alpha = 5.061*(Hmo^2/Tp^4)*(1-0.287*log(gamma));
```

```
30 -        Sj = ((alpha.*9.81.^2)./(w.^5)).*exp(-(5/4).*(3.5./w).^4).*gamma.^exp((-(w./3.5-1).^2)./(2.*0.07.^2));
31 -        T = (2.*pi())./w;
32
33 -        M = trapz((af.*Sj)./T.^2);
34 -        D = trapz(bf.*Sj.*T);
35 -        E = trapz(FefA.*Sj'.*sin(Fefph));
36
37 -        coeff = [0.4; -0.1; 0.2];
38 -        Proxy = M.*coeff(1)+D.*coeff(2)+E.*coeff(3);
39
40 -    end
```

GA_shapes_v2.m | objfunShapes2.m | axiMeshGA2.m | NemohEval.m | NemohGA2.m

```
1   %
2   % --> function [A,B,Fe]=Nemoh(w, dir, depth)
3   %
4   % Purpose: Matlab wrapper for calculation of hydrodynamic coefficients using Nemoh
5   %
6   % Inputs :
7   % - w     : Vector length(w) of wave frequencies (rad/s)
8   % - dir   : Wave direction (degrees)
9   % - depth : water depth (m), 0 for deep water.
10  %
11  % Outputs :
12  % - A  : Matrix (6xnBodies)x(6xnBodies)xlength(w) of added mass coefficients
13  % - B  : Matrix (6xnBodies)x(6xnBodies)xlength(w) of radiation damping coefficients
14  % - Fe : Matrix (6xnBodies)xlength(w) of exciation forces (complex
15  % values)
16  %
17  % Copyright Ecole Centrale de Nantes 2014
18  % Licensed under the Apache License, Version 2.0
19  % Written by A. Babarit, LHEEA Lab.
20  %
21  function [A,B,Fe]=Nemoh(w,p)
22  % Preparation du calcul
23  dir=180;    %head on
24  depth=0;    %unlimited depth
25  name=sprintf('%d',p);   %Individuals in a population are saved in separate folders, repeated each gen
26  fid=fopen(fullfile('C:\Users\labuser\Documents\Kaylie\GA\100GenParallel\',name,'ID.dat'));       %change all to \nomrep\nomrep
27  line=fgetl(fid);
28  rep=fscanf(fid,'%s',1);
29  fclose('all');
```